Active rejection control for unknown harmonic disturbances of the transverse deflection of steel strips with control input, system output, sensor output, and disturbance input at different positions

authored by **M. Saxinger, L. Marko, A. Steinboeck, and A. Kugi**

and published in *Mechatronics*.

Contact:

Automation and Control Institute (ACIN)
TU Wien
Gusshausstrasse 27-29/E376
1040 Vienna, Austria

Internet: www.acin.tuwien.ac.at
E-mail: office@acin.tuwien.ac.at
Phone: +43 1 58801 37601
Fax: +43 1 58801 37699

Active rejection control for unknown harmonic disturbances of the transverse deflection of steel strips with control input, system output, sensor output, and disturbance input at different positions

Martin Saxinger[a,*], Lukas Marko[a], Andreas Steinboeck[b], Andreas Kugi[a]

[a] *Christian Doppler Laboratory for Model-Based Process Control in the Steel Industry, Automation and Control Institute, TU Wien, Gußhausstraße 27-29 / E376, 1040 Vienna, Austria*
[b] *Automation and Control Institute, TU Wien, Gußhausstraße 27-29 / E376, 1040 Vienna, Austria*

Abstract

In hot-dip galvanizing lines for steel strips, it is important to ensure a homogeneous zinc layer thickness. For this, vibrations of the strip at the gas wiping dies, where excess liquid zinc is blown off, must be suppressed. These vibrations typically exhibit a dominant sinusoidal shape and the excitation process, the frequency, the amplitude, and the phase are generally unknown.

In modern plants, electromagnetic actuators are employed to enable a contactless vibration and shape control of the steel strip. Vibration control of flexible structures is well established in literature. However, in the considered application the disturbance (source of periodic excitation), the control input (force of electromagnetic actuators), the sensor output (strip displacement) and the desired system output (strip displacement at the gas wiping dies) are all located at different positions along the strip, which makes the overall control task quite challenging. In this paper, a control concept consisting of a linear quadratic regulator combined with a disturbance feedforward concept based on the theory of invariant manifolds and an Extended Kalman Filter is developed. The proposed control strategy is successfully tested on an experimental test rig for different scenarios.

Keywords: Distributed-parameter system, disturbance rejection, internal model principle, periodic signals, active vibration control, steel industry

1. Introduction

1.1. Problem description and motivation for this work

Figure 1 outlines a sketch of an industrial hot-dip galvanizing line for steel strips. In such plants, steel strips are coated in a bath of molten zinc. Excess liquid zinc is blown off by so-called gas wiping dies. To get a homogeneous zinc layer thickness, the supply pressure of the gas wiping dies must be constant and the distance between the gas wiping dies and the strip (air gap) must be both constant and uniform in lateral direction. Clearly, vibrations of the strip lead to fluctuations in the air gap and thus a deterioration of the product quality due to an inhomogeneous zinc layer. Vibrations of the strip can originate from different sources, e.g., air jets at the gas wiping dies and air jets in the cooling section of the hot-dip galvanizing line [1, 2, 3]. In view of the multiple actuators and rolls along the plant, maintaining a constant tensile force in the strip is known to be a challenging task. Fluctuations of the tensile force in the strip can also lead to transversal strip vibrations. Eccentric rolls in the zinc bath or eccentric touch rolls above the gas wiping dies are a frequently encountered source of vibrations [4, 5]. A typical amplitude spectrum of a transverse displacement measurement at a hot-dip galvanizing line of voestalpine Stahl GmbH in Linz, Austria, see also [6], is shown in Fig. 2. Here, the frequency of the measured transverse strip displacement clearly coincides with the rotating frequency of a zinc bath roll, i.e., the correction roll. It can be assumed that these disturbances have approximately a sinusoidal shape, see Fig. 2. Typically, either the correction roll or the stabilization roll, which both have nearly the same diameter, cause these disturbances. In our case, the sink roll, which has a large diameter, was never observed as origin of the disturbances. In general, the mechanism behind the periodic disturbances and the exact excitation process are not known. Therefore, it is reasonable to assume that the disturbance acts somewhere on the strip, is periodic, and has an unknown frequency, amplitude, and phase. For vibration damping and shape control, newer plants are equipped with electromagnetic actuators, which are located some distance above the gas wiping dies, see, e.g., [7, 8]. Moreover, displacement sensors are often located nearby the electromagnetic actua-

*Corresponding author
Email addresses: saxinger@acin.tuwien.ac.at (Martin Saxinger), marko@acin.tuwien.ac.at (Lukas Marko), steinboeck@acin.tuwien.ac.at (Andreas Steinboeck), kugi@acin.tuwien.ac.at (Andreas Kugi)

Post-print version of the article: M. Saxinger, L. Marko, A. Steinboeck, and A. Kugi, "Active rejection control for unknown harmonic disturbances of the transverse deflection of steel strips with control input, system output, sensor output, and disturbance input at different positions", *Mechatronics*, vol. 56, pp. 73–86, 2018, ISSN: 0957-4158. DOI: 10.1016/j.mechatronics.2018.10.008
The content of this post-print version is identical to the published paper but without the publisher's final layout or copy editing.

tors. However, they are typically not perfectly collocated, mainly due to space restrictions. Thus, we are confronted with the situation that the disturbance input (Ⓘ, source of periodic excitation of the strip), the control input (Ⓘ, force of the electromagnetic actuators), the sensor output (Ⓘ, transverse strip displacement sensor), and the system output (Ⓘ, transverse strip displacement in the gas wiping dies) are all located at different positions along the strip. For such a configuration, it is well known that vibration damping in the system output is quite challenging. For the development of the overall control strategy, an experimental test rig according to Fig. 3 was designed to be able to easily study different control concepts and the influence of different actuator and sensor positions. Clearly, the test rig of Fig. 3 is a simplified representation of the conditions in the real plant according to Fig. 1. The test rig captures the main effects necessary for the design of a robust and feasible vibration damping strategy. The positions Ⓘ to Ⓘ in Fig. 3 correspond to those in Fig. 1. In the experimental test rig, cf. Fig. 3, Ⓘ is the position of a disturbance actuator, the transversal strip displacement at the position Ⓘ is the system output, the electromagnetic actuator at the position Ⓘ is used as the control input, and Ⓘ is the position of the (single) sensor output used for the observer. The moderate longitudinal bulk velocities of the strips (main strip transport) in industrial hot-dip galvanizing lines only have a minor influence on the transverse strip dynamics. Hence, neglecting the strip transport in longitudinal direction in the experimental test rig is justified. However, similar to the hot-dip galvanizing line, the tensile load N_{xx} in the strip of the experimental test rig can be accurately adjusted. The remaining laser distance sensors in the experimental test rig are only used for visualization of the strip shape during the experiments.

1.2. State of the art in vibration control of flexible structures

In the first place, PID controllers are often used for active damping control in hot-dip galvanizing lines equipped with electromagnetic actuators, see, e.g., [9]. More complex control algorithms, e.g., positive position feedback as described in [10] or passive damping and boundary control as reported in [11], are also proposed for vibration damping in hot-dip galvanizing lines. More recently, electromagnetic actuators are also applied to rectify flatness defects in strips to improve the quality of the lateral zinc profiles. In [8], electromagnetic actuators were used for both vibration control and the regulation of a uniform lateral zinc profile.

Active vibration control of flexible structures like strings, beams, plates, and shells has been an active field of research in the last decades, see, e.g., [12, 13]. Most of these control strategies require collocation of the sensor-actuator pair. In [14], a magnetic suspension system is described, which is used for non-contact processing and vibration control of tubular beams. More recently, a vibration control method for a clamped-clamped aluminum beam using a multi positive feedback control was demonstrated in [15]. In some applications, however, collocation of the sensor-actuator pair is not feasible, e.g. due to space restrictions. Especially for systems with very low structural damping, e.g., thin metal strips, it is hard to achieve a stable control loop in case of non-collocated sensor-actuator configurations, see, e.g., [16]. However, active vibration control with non-collocated sensor-actuator configuration has been demonstrated in different publications, see, e.g., [17, 18, 19]. H_2, H_∞, and μ-synthesis methods are used for the synthesis of optimal and robust controllers with guaranteed performance [20]. In [21], a review of H_∞ and μ-synthesis methods for both collocated and non-collocated sensor-actuator pairs for the active vibration control in flexible structures like beams and plates can be found. Moreover, LQR and LQG methods are also well established for active vibration control in flexible structures like beams, see, e.g., [13].

Periodic disturbances are a frequently observed phenomenon in machines with rotating parts. The most obvious solution would be to eliminate the disturbance itself. If this cannot be realized, the difficulty of rejecting periodic disturbances depends on the structure of the considered system. The rejection of a sinusoidal disturbance at a position which coincides with the position of a sensor and an actuator is a relatively simple problem. Here, disturbance rejection control is even possible without a mathematical model of the system. There are many publications addressing the so-called filtered-X LMS algorithm for minimizing the least mean square of a measured error signal, see, e.g., [22, 23]. An overview of narrow-band disturbance rejection control with known frequency is given, e.g., in [24, 25]. An overview of disturbance rejection methods for both known and unknown frequencies of the periodic disturbance can be found, e.g., in [26]. Most of these methods can only reject the disturbance at a position, which is measured by a displacement sensor. In [27], disturbance rejection is demonstrated for a known frequency. Here, a sinusoidal disturbance in an optical disc drive due to disc eccentricity is considered. The disturbance is rejected by an additional controller which is added to the existing feedback controller. This method was extended in [28] to deal with a sinusoidal disturbance with non-zero mean. The frequency is estimated by an additional adaption algorithm. Another extension for frequency estimation was published in [29]. In [30], an algorithm for adaptive disturbance rejection in a MIMO system is presented. Furthermore, a compensator with an adaptive internal model for the rejection of sinusoidal disturbances based on measurements of the tracking error is given in [31]. In [32], a nonlinear disturbance observer is proposed, where the disturbance is excited by a linear exogenous system. The disturbance observer design is separated from the controller design and it is assumed that the states of the nonlinear system are known. The control method is applied to a robotics application. In [33], a method for the solution of an output regulation problem for a linear distributed-parameter sys-

Post-print version of the article: M. Saxinger, L. Marko, A. Steinboeck, and A. Kugi, "Active rejection control for unknown harmonic disturbances of the transverse deflection of steel strips with control input, system output, sensor output, and disturbance input at different positions", *Mechatronics*, vol. 56, pp. 73–86, 2018, ISSN: 0957-4158. DOI: 10.1016/j.mechatronics.2018.10.008
The content of this post-print version is identical to the published paper but without the publisher's final layout or copy editing.

tem is considered, where a so-called dual observer is used and the system outputs to be controlled are not measured. In a simulation study, the method is tested for the rejection of a sinusoidal disturbance with a constant and known frequency at a certain position of an Euler-Bernoulli beam, where an ideal and pointlike actuator force is considered as system input.

This work deals with the rejection of an unmeasured transverse vibration of a steel strip under tensile load at a certain position (gas wiping dies). The vibration of the strip is excited by an unknown sinusoidal disturbance (with unknown frequency) at one end of the strip. Custom-made magnetic actuators are used to exert a desired force without measuring the gap between the strip and the core. A direct measurement of the force acting on the strip is not necessary. Hence, the quasi-static force characteristics of the magnet is used. The states of both the strip and the disturbance are observed by an Extended Kalman Filter [34], which uses just one displacement sensor as a measurement output and a magnetic actuator (at a different position) as a control input. A combination of an optimal state controller and an additional controller for disturbance rejection, which is based on the principle of invariant manifolds, is applied [35, 36, 37]. In general, one actuator allows the rejection of the disturbance at one certain point of the strip. Nominal parameters of the strip, e.g., mechanical parameters, tensile load, and the boundary conditions are known with sufficient accuracy. This is also true for the force characteristics of the magnetic actuator. The feasibility and robustness of the developed control method are tested by means of an experimental rig. This rig and the current work serve as the basis for the implementation of the method in an industrial hot-dip galvanizing line. An adaption of the finite element model to the dimensions of the hot-dip galvanizing line is possible without significant effort [38, 39].

Remark: High temperatures and dust consisting of zinc and other alloy particles in the vicinity of the zinc pot constitute harsh conditions for sensors and actuators. In order to prevent inaccuracies or failures of these devices, they are usually placed in a housing with special heat shields, active air cooling, and mechanical protection. Besides the protection of the sensors and actuators against overheating, increased temperatures do also influence the magnetic properties of both the magnetic cores and the strip. This affects the magnetic force applied to the strip, see also [7]. Fortunately, the longitudinal temperature profile of the strip in the hot-dip galvanizing line is well known and can be taken into account. Actually, there are two methods for considering the temperature influence on the magnetic force. First, a finite element model can be used for up-front calculations of the quasi-static magnetic forces. These forces are calculated as a function of different air gaps, coil currents, and strip thicknesses and are stored in a look-up table. Here, the mathematical model has to take into account the dependence of the B-H curve (magnetic properties) of the strip on the temperature. Note that the temperature influence on the magnetic properties in different materials is well investigated [40]. As a second possibility, the quasi-static magnetic forces can be directly measured for different air gaps, coil currents, strip thicknesses, and strip temperatures using a special test rig. Based on these measurements, the look-up tables can be generated. Such a test rig must be equipped with a force sensor, a strip heating device, and a controller for the specimen (steel strip) temperature.

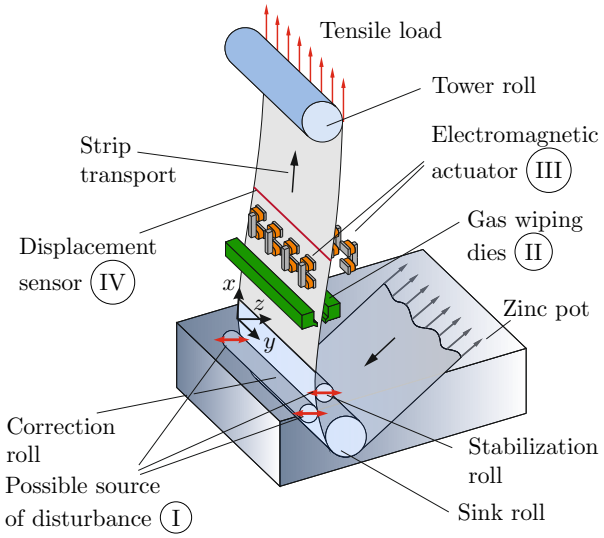

Figure 1: Typical hot-dip galvanizing line for steel strips.

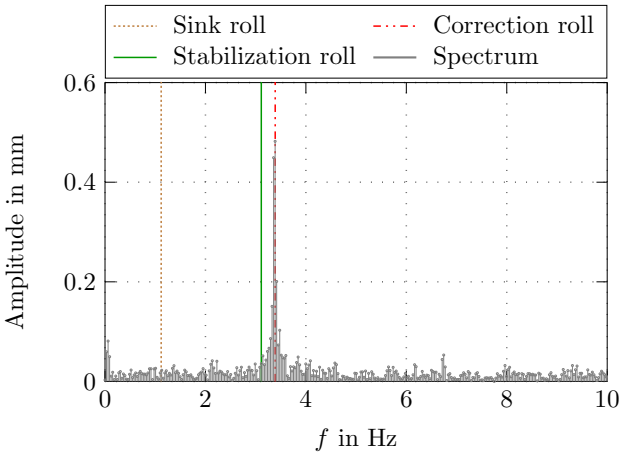

Figure 2: Typical single-sided amplitude spectrum of a measured strip displacement.

2. Mathematical model

In this section, the mathematical model of the steel strip in the test rig according to Fig. 3 is derived. The strip has

Post-print version of the article: M. Saxinger, L. Marko, A. Steinboeck, and A. Kugi, "Active rejection control for unknown harmonic disturbances of the transverse deflection of steel strips with control input, system output, sensor output, and disturbance input at different positions", *Mechatronics*, vol. 56, pp. 73–86, 2018, ISSN: 0957-4158. DOI: 10.1016/j.mechatronics.2018.10.008
The content of this post-print version is identical to the published paper but without the publisher's final layout or copy editing.

the length L, the width b, the thickness h, and the mass density ρ. Both ends of the strip are cantilever-mounted. As the width b of the strip is small compared to its length L, the strip can be regarded as a beam. A slowly time-varying sinusoidal disturbance in the form of a displacement $w^d(t)$ is prescribed by the disturbance actuator at the boundary $x = 0$. At the boundary $x = L$, a constant tensile load N_{xx} is ensured by an actively controlled slide. The transversal displacement of the strip (measured at its center line) is denoted by $w = w(x,t)$. Gravity acts along the direction y and hence does not influence the transverse strip displacement. Air resistance at the strip surface is assumed to cause viscous damping with the coefficient c. A viscoelastic material behavior of the strip is considered. A transversal load due to the electromagnetic actuator acts on the strip and is denoted by $q = q(x,t)$. Based on the assumption of a uniform distribution of the electromagnetic force, q can be written in the form

$$q(x,t) = \begin{cases} \frac{F^m(t)}{\Delta x_m} & \text{for } x_{m,l} \leq x \leq x_{m,u} \\ 0 & \text{else,} \end{cases} \tag{1}$$

where the resultant magnetic force F^m serves as control input. The positions $x_{m,l} = x_m - \frac{\Delta x_m}{2}$ and $x_{m,u} = x_m + \frac{\Delta x_m}{2}$ are indicated in Fig. 3. An additional unknown transversal load $p = p(x,t)$, which will be useful in the observer design, is considered.

2.1. Equations of motion

In [41], mathematical models of plates and beams are developed applying the Kirchhoff-Love hypothesis. With the assumptions made in this section, the equations of motion can be written as

$$\rho b h \partial_t^2 w - \partial_x^2 M_{xx} - N_{xx}\partial_x^2 w - (q+p) + c\partial_t w = 0, \tag{2}$$

with the transversal displacement w. This equation is defined in the range $x \in (0, L)$. The first expression in (2) is the inertia term, the expressions involving the bending moment M_{xx} and the tensile load N_{xx} describe the stiffness against the displacement w. The contribution of the transversal loads and the viscous damping force is considered in the last three terms. In order to obtain (2), a free lateral contraction is assumed along the boundaries of the strip. The stress-strain relation according to Hooke's law extended by a Kelvin-Voigt material damping yields the bending moment in the form

$$M_{xx} = -D\big(\partial_x^2 w + \lambda \partial_t \partial_x^2 w\big) \tag{3}$$

with $D = EI$. Here, E is Young's modulus, and $I = \frac{bh^3}{12}$ is the moment of inertia. In (3), λE denotes the Kelvin-Voigt damping factor. The parameters λ and E are assumed to be uniform along the strip. Based on the previous assumptions, the boundary conditions are given by

$$w(0,t) = w^d(t) \tag{4a}$$
$$\partial_x w(0,t) = 0 \tag{4b}$$
$$w(L,t) = 0 \tag{4c}$$
$$\partial_x w(L,t) = 0. \tag{4d}$$

The initial conditions take the form

$$w(x,0) = w_0(x) \tag{5a}$$
$$\partial_t w(x,0) = w_1(x) \tag{5b}$$

for $x \in [0, L]$. They must be consistent with the boundary conditions (4).

2.2. Spatial discretization

In the following, a finite-dimensional approximation is performed by applying Galerkin's weighted residual method to the mathematical model (2)-(5). The strip length is discretized into n finite elements, where the length of a local element $e \in \{1, \ldots, n\}$ is denoted by a_e. To accurately compute the shape and motion of the strip in the vicinity of the boundaries $x = 0$ and $x = L$, the elements are chosen smaller in this region compared to the rest of the domain. Local trial functions are assembled in the vector

$$\boldsymbol{\Psi}_e(\tilde{x}_e) = \big[\Psi^w_{e-1,e}(\tilde{x}_e), \Psi^{\partial w}_{e-1,e}(\tilde{x}_e), \Psi^w_{e,e+1}(\tilde{x}_e), \Psi^{\partial w}_{e,e+1}(\tilde{x}_e)\big]^{\mathrm{T}}$$

with Hermite polynomials of the form

$$\Psi^w_{e-1,e}(\tilde{x}_e) = 2\tilde{x}_e^3/a_e^3 - 3\tilde{x}_e^2/a_e^2 + 1 \tag{6a}$$
$$\Psi^{\partial w}_{e-1,e}(\tilde{x}_e) = -\tilde{x}_e^3/a_e^2 + 2\tilde{x}_e^2/a_e - \tilde{x}_e \tag{6b}$$
$$\Psi^w_{e,e+1}(\tilde{x}_e) = -2\tilde{x}_e^3/a_e^3 + 3\tilde{x}_e^2/a_e^2 \tag{6c}$$
$$\Psi^{\partial w}_{e,e+1}(\tilde{x}_e) = -\tilde{x}_e^3/a_e^2 + \tilde{x}_e^2/a_e \tag{6d}$$

for $\tilde{x}_e \in [0, a_e]$. The time-dependent vector of the Galerkin coefficients of an element e can be written as

$$\tilde{\mathbf{T}}_e = \big[T^w_{e-1,e}, \quad T^{\partial w}_{e-1,e}, \quad T^w_{e,e+1}, \quad T^{\partial w}_{e,e+1}\big]^{\mathrm{T}} \tag{7}$$

and the approximated transversal displacement is given by

$$w = (\boldsymbol{\Psi}_e(\tilde{x}_e))^{\mathrm{T}} \tilde{\mathbf{T}}_e(t)$$

for the local element e. The entries in (7) have the following meaning: $T^w_{e-1,e}$ and $T^w_{e,e+1}$ describe the displacement of the strip at the local positions $\tilde{x}_e = 0$ and $\tilde{x}_e = a_e$, respectively. $T^{\partial w}_{e-1,e}$ and $T^{\partial w}_{e,e+1}$ define the slopes of the strip at the positions $\tilde{x}_e = 0$ and $\tilde{x}_e = a_e$. The distributed load p is introduced in the form

$$p = (\boldsymbol{\Upsilon}_e(\tilde{x}_e))^{\mathrm{T}} \tilde{\mathbf{p}}_e(t),$$

where

$$\boldsymbol{\Upsilon}_e(\tilde{x}_e) = \big[\Psi^w_{e-1,e}(\tilde{x}_e), \Psi^w_{e,e+1}(\tilde{x}_e)\big]^{\mathrm{T}}$$

Post-print version of the article: M. Saxinger, L. Marko, A. Steinboeck, and A. Kugi, "Active rejection control for unknown harmonic disturbances of the transverse deflection of steel strips with control input, system output, sensor output, and disturbance input at different positions", *Mechatronics*, vol. 56, pp. 73–86, 2018, ISSN: 0957-4158. DOI: 10.1016/j.mechatronics.2018.10.008

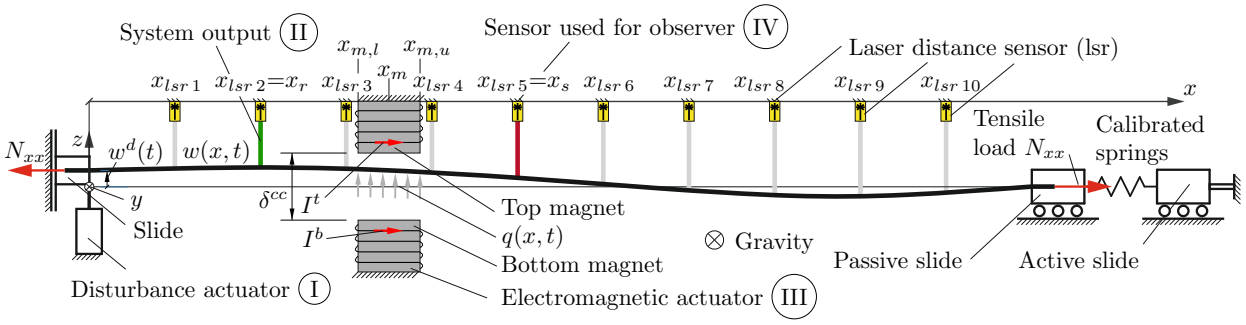

Figure 3: Experimental test rig of the clamped steel strip.

and

$$\tilde{\mathbf{p}}_e = \left[p^w_{e-1,e}, p^w_{e,e+1}\right]^{\mathrm{T}} \tag{8}$$

are used. In (8), $p^w_{e-1,e}$ and $p^w_{e,e+1}$ represent the transversal loads at the boundaries $\tilde{x}_e = 0$ and $\tilde{x}_e = a_e$ of the finite element e, respectively. Similar to [38, 39], the equations of motion for an element $e = 2, \ldots, n-1$ can be written in matrix form as

$$\tilde{\mathbf{M}}_e \ddot{\tilde{\mathbf{T}}}_e + \tilde{\mathbf{D}}_e \dot{\tilde{\mathbf{T}}}_e + \tilde{\mathbf{K}}_e \tilde{\mathbf{T}}_e = \tilde{\mathbf{F}}^q_e + \tilde{\mathbf{H}}^p_e \tilde{\mathbf{p}}_e, \tag{9}$$

with the mass matrix $\tilde{\mathbf{M}}_e$, the stiffness matrix $\tilde{\mathbf{K}}_e = \tilde{\mathbf{K}}^M_e + \tilde{\mathbf{K}}^N_e$, the damping matrix $\tilde{\mathbf{D}}_e$, the abbreviations

$$\tilde{\mathbf{M}}_e = \rho b h \int_0^{a_e} \mathbf{\Psi}_e \mathbf{\Psi}_e^{\mathrm{T}} \mathrm{d}\tilde{x}_e \tag{10a}$$

$$\tilde{\mathbf{K}}^M_e = D \int_0^{a_e} \partial_x^2 \mathbf{\Psi}_e \left(\partial_x^2 \mathbf{\Psi}_e\right)^{\mathrm{T}} \mathrm{d}\tilde{x}_e \tag{10b}$$

$$\tilde{\mathbf{K}}^N_e = N_{xx} \int_0^{a_e} (\partial_x \mathbf{\Psi}_e)(\partial_x \mathbf{\Psi}_e)^{\mathrm{T}} \mathrm{d}\tilde{x}_e \tag{10c}$$

$$\tilde{\mathbf{F}}^q_e = \int_0^{a_e} \mathbf{\Psi}_e q \mathrm{d}\tilde{x}_e \tag{10d}$$

$$\tilde{\mathbf{H}}^p_e = \int_0^{a_e} \mathbf{\Psi}_e \mathbf{\Upsilon}_e^{\mathrm{T}} \mathrm{d}\tilde{x}_e, \tag{10e}$$

and $\dot{(\cdot)}$ for time derivatives. In (10), $\tilde{\mathbf{K}}^M_e$ is a matrix describing the bending stiffness, and the matrix $\tilde{\mathbf{K}}^N_e$ represents the stiffness due to the tensile load N_{xx}. Transversal loads q caused by the electromagnetic actuator are taken into account in the vector $\tilde{\mathbf{F}}^q_e$. The matrix $\tilde{\mathbf{H}}^p_e$ is employed for considering the distributed load p. In (9), $\tilde{\mathbf{D}}_e = \mu \tilde{\mathbf{M}}_e + \lambda \tilde{\mathbf{K}}^M_e$ constitutes a Rayleigh damping formulation for outer viscous and internal material damping, see, e.g., [42]. Here, $\mu \tilde{\mathbf{M}}_e$ with the abbreviation $\mu = \frac{c}{\rho b h}$ is the damping matrix due to viscous air friction, and $\lambda \tilde{\mathbf{K}}^M_e$ is the damping matrix caused by material damping.

2.3. Finite-dimensional model

For the elements $e = 1$ and $e = n$, the boundary conditions (4) have to be implemented based on (7) and (6). This yields $T^w_{0,1} = w^d(t)$, $T^{\partial w}_{0,1} = 0$, $T^w_{n,n+1} = 0$, and $T^{\partial w}_{n,n+1} = 0$. Thus, assembling the equations of motion (9) for all elements $e = 1, \ldots, n$, we get $\bar{n} = 2(n-1)$ independent Galerkin coefficients

$$\mathbf{T} = \left[T^w_{1,2}, \quad T^{\partial w}_{1,2} \quad , \ldots, \quad T^w_{n-1,n}, \quad T^{\partial w}_{n-1,n}\right]^{\mathrm{T}}$$

and the equations of motion read as

$$\hat{\mathbf{M}}\ddot{\mathbf{T}} + \hat{\mathbf{D}}\dot{\mathbf{T}} + \hat{\mathbf{K}}\mathbf{T} = \hat{\mathbf{B}}F^m + \hat{\mathbf{H}}^p\mathbf{p} - \hat{\mathbf{G}}^K w^d - \hat{\mathbf{G}}^D \dot{w}^d - \hat{\mathbf{G}}^M \ddot{w}^d. \tag{11}$$

Here, $\hat{\mathbf{M}}$, $\hat{\mathbf{D}}$, and $\hat{\mathbf{K}}$ refer to the assembled mass, damping, and stiffness matrices, respectively, and the vectors $\hat{\mathbf{G}}^K$, $\hat{\mathbf{G}}^D$, and $\hat{\mathbf{G}}^M$ correspond to the expressions with $T^w_{0,1}$ in (9). Moreover, $\hat{\mathbf{B}}F^m$ refers to the assembled vector $\tilde{\mathbf{F}}^q_e$ from (10d) with q replaced by (1). $\hat{\mathbf{H}}^p\mathbf{p}$, with $\mathbf{p} = [p^w_{1,2}, \ldots, p^w_{n-1,n}]^{\mathrm{T}}$, follows from (10e) for all elements $e = 2, \ldots, n-1$ with the assumption $p^w_{0,1} = p^w_{n,n+1} = 0$.

Remark: The latter assumption implies that the additional transversal load $p(x,t)$ decays within the boundary elements and is zero at $x = 0$ and $x = L$. This is not really a restriction of the mathematical model because the transversal displacements at $x = 0$ and $x = L$ are prescribed and thus not influenced by the quantities $p^w_{0,1}$ and $p^w_{n,n+1}$. Moreover, the lengths of the boundary elements are small compared to the other elements meaning that the approximation error is just local. However, the assumption is particularly beneficial for the implementation of the mathematical strip model.

Henceforth, the expressions

$$w^s = \left(\hat{\mathbf{C}}^s\right)^{\mathrm{T}}\mathbf{T}, \quad w^r = \left(\hat{\mathbf{C}}^r\right)^{\mathrm{T}}\mathbf{T}, \quad w^m = \left(\hat{\mathbf{C}}^m\right)^{\mathrm{T}}\mathbf{T},$$

denote the transversal strip displacement at the positions $x = x_s$ of the displacement sensor, $x = x_r$ of the system output, and $x = x_m$ of the electromagnetic actuator, respectively. Let $\tilde{x}^\chi_e$, $\chi \in \{s, r, m\}$ be a position within the corresponding finite element ξ_χ. Then $\hat{\mathbf{C}}^\chi$ takes the form

$$\hat{\mathbf{C}}^\chi = \Big[0, \ldots, 0, \Psi^w_{\xi_\chi - 1, \xi_\chi}(\tilde{x}^\chi_e), \Psi^{\partial w}_{\xi_\chi - 1, \xi_\chi}(\tilde{x}^\chi_e), \Psi^w_{\xi_\chi, \xi_\chi + 1}(\tilde{x}^\chi_e), \Psi^{\partial w}_{\xi_\chi, \xi_\chi + 1}(\tilde{x}^\chi_e), 0, \ldots, 0\Big]^{\mathrm{T}}. \tag{12}$$

Post-print version of the article: M. Saxinger, L. Marko, A. Steinboeck, and A. Kugi, "Active rejection control for unknown harmonic disturbances of the transverse deflection of steel strips with control input, system output, sensor output, and disturbance input at different positions", *Mechatronics*, vol. 56, pp. 73–86, 2018, ISSN: 0957-4158. DOI: 10.1016/j.mechatronics.2018.10.008
The content of this post-print version is identical to the published paper but without the publisher's final layout or copy editing.

For the following investigations, we consider a sinusoidal disturbance $w^d(t)$ with unknown but constant frequency ω. Thus, the exogenous disturbance model can be written in the form

$$\dot{\mathbf{w}}^d = \mathbf{A}^d(\omega)\mathbf{w}^d, \qquad \mathbf{w}_0^d = \mathbf{w}^d(0) \tag{13a}$$

$$\mathbf{w}^d = \begin{bmatrix} w^d & \dot{w}^d \end{bmatrix}^{\mathrm{T}} \tag{13b}$$

$$\mathbf{A}^d(\omega) = \begin{bmatrix} 0 & 1 \\ -\omega^2 & 0 \end{bmatrix}. \tag{13c}$$

Remark: The assumption of a constant frequency ω does not constitute a considerable restriction for the considered application. In industrial hot-dip galvanizing lines, strips are welded together to ensure a continuous operation of the processing line. For quality reasons, the longitudinal bulk velocity of the strips has to be kept constant and is only allowed to be slowly changed if a welded joint traverses the plant. Because roll eccentricities are one of the main sources for the periodic disturbances, also the disturbance frequency is constant for most of the times and changes only slowly in transition periods. A slow change of the frequency ω can be well captured by the control method presented in this paper, as will also be demonstrated by the experimental results in Section 5.

Introducing the state vector $\mathbf{x}^{\mathrm{T}} = \begin{bmatrix} \mathbf{T}^{\mathrm{T}} & \dot{\mathbf{T}}^{\mathrm{T}} \end{bmatrix}$ and substituting $\ddot{w}^d(t)$ from (13) into (11) finally yields the state-space representation of the strip model

$$\dot{\mathbf{x}} = \mathbf{A}\mathbf{x} + \mathbf{B}u + \mathbf{G}(\omega)\mathbf{w}^d + \mathbf{H}\mathbf{p}, \qquad \mathbf{x}_0 = \mathbf{x}(0) \tag{14a}$$

$$y = (\mathbf{C}^r)^{\mathrm{T}}\mathbf{x}, \tag{14b}$$

with the control input $u = F^m$, the system output $y = w^r$,

$$\mathbf{A} = \begin{bmatrix} \mathbf{0}^{\bar{n}\times\bar{n}} & \mathbf{I}^{\bar{n}\times\bar{n}} \\ -\hat{\mathbf{M}}^{-1}\hat{\mathbf{K}} & -\hat{\mathbf{M}}^{-1}\hat{\mathbf{D}} \end{bmatrix}, \qquad \mathbf{B} = \begin{bmatrix} \mathbf{0}^{\bar{n}\times 1} \\ \hat{\mathbf{M}}^{-1}\hat{\mathbf{B}} \end{bmatrix} \tag{15a}$$

$$\mathbf{H} = \begin{bmatrix} \mathbf{0}^{\bar{n}\times n-1} \\ \hat{\mathbf{M}}^{-1}\hat{\mathbf{H}}^p \end{bmatrix} \tag{15b}$$

$$\mathbf{G}(\omega) = \begin{bmatrix} \mathbf{0}^{\bar{n}\times 1} & \mathbf{0}^{\bar{n}\times 1} \\ -\hat{\mathbf{M}}^{-1}\left(\hat{\mathbf{G}}^K - \omega^2\hat{\mathbf{G}}^M\right) & -\hat{\mathbf{M}}^{-1}\hat{\mathbf{G}}^D \end{bmatrix} \tag{15c}$$

$$\mathbf{C}^r = \begin{bmatrix} \left(\hat{\mathbf{C}}^r\right)^{\mathrm{T}} & \mathbf{0}^{1\times\bar{n}} \end{bmatrix}^{\mathrm{T}}, \tag{15d}$$

and the identity matrix $\mathbf{I}$. The complete plant model consists of (13) and (14). The discrete-time representation of the (linear) system (13), (14) for the sampling time T_s can be calculated in the form

$$\mathbf{x}_{k+1} = \mathbf{\Phi}\mathbf{x}_k + \mathbf{\Gamma}u_k + \mathbf{\Delta}(\omega_k)\mathbf{w}_k^d + \mathbf{\Sigma}\mathbf{p}_k, \ \mathbf{x}_0 = \mathbf{x}(0) \tag{16a}$$

$$\mathbf{w}_{k+1}^d = \mathbf{\Phi}^d(\omega_k)\mathbf{w}_k^d, \qquad \mathbf{w}_0^d = \mathbf{w}^d(0) \tag{16b}$$

$$\omega_{k+1} = \omega_k, \qquad \omega_0 = \omega(0) \tag{16c}$$

$$y_k = (\mathbf{C}^r)^{\mathrm{T}}\mathbf{x}_k \tag{16d}$$

$$\mathbf{\Phi} = \exp(\mathbf{A}T_s), \qquad \mathbf{\Phi}^d(\omega_k) = \exp\big(\mathbf{A}^d(\omega_k)T_s\big) \tag{16e}$$

$$\mathbf{\Gamma} = \int_0^{T_s} \exp(\mathbf{A}\tau)\mathrm{d}\tau\mathbf{B} \tag{16f}$$

$$\mathbf{\Delta}(\omega_k) = \int_0^{T_s} \exp(\mathbf{A}\tau)\mathbf{G}(\omega_k)\exp\big(\mathbf{A}^d(\omega_k)(T_s-\tau)\big)\mathrm{d}\tau \tag{16g}$$

$$\mathbf{\Sigma} = \int_0^{T_s} \exp(\mathbf{A}\tau)\mathrm{d}\tau\mathbf{H}. \tag{16h}$$

Here the index k refers to the time instant $t = kT_s$.

3. Vibration control strategy

In a first step, a control strategy will be designed under the assumption that the whole state information of the system (16a), of the exogenous disturbance (16b), and of the frequency (16c) is available. The control design is based on a combination of a linear quadratic regulator (LQR) for the suppression of broad-band disturbances and a disturbance feedforward concept, which exploits the theory of invariant manifolds and is tailored to the rejection of sinusoidal disturbances (narrow-band disturbance), see, e.g., [35, 36, 37, 43]. Because the transversal displacement can be measured at only one position, see sensor output at the point x_s in Fig. 3, an observer concept will be employed in a second step.

3.1. Controller design

In (16), $\mathbf{p}_k$ is set to zero for the controller design. Because, the disturbance frequency ω is constant or only slowly varying and the frequency is estimated by a state observer, it is reasonable to consider $\omega_k = \omega(kT_s)$ to be known and constant for each sampling interval $kT_s \le t < (k+1)T_s$. Therefore, the exogenous disturbance model (13) is neutral stable, which means that all eigenvalues of $\mathbf{A}^d(\omega_k)$ are on the imaginary axis, see, e.g., [26, 44].

Now, we propose the control law

$$u_k = \underbrace{(\mathbf{K}^x)^{\mathrm{T}}\mathbf{x}_k}_{u_k^x} + (\mathbf{K}^w)^{\mathrm{T}}\mathbf{w}_k^d, \tag{17}$$

where the feedback gains $\mathbf{K}^x \in \mathbb{R}^{2\bar{n}}$ and $\mathbf{K}^w \in \mathbb{R}^2$ have to be properly designed. The feedback gain $\mathbf{K}^x$ results from the solution of the LQR problem for the cost function

$$J(\mathbf{x}_0) = \sum_{k=0}^{\infty}\left(\mathbf{x}_k^{\mathrm{T}}\mathbf{Q}\mathbf{x}_k + u_k^x R u_k^x\right), \tag{18}$$

Post-print version of the article: M. Saxinger, L. Marko, A. Steinboeck, and A. Kugi, "Active rejection control for unknown harmonic disturbances of the transverse deflection of steel strips with control input, system output, sensor output, and disturbance input at different positions", *Mechatronics*, vol. 56, pp. 73–86, 2018, ISSN: 0957-4158. DOI: 10.1016/j.mechatronics.2018.10.008

with the positive semi-definite weighting matrix $\mathbf{Q}$ and the weighting factor $R > 0$, subject to the constraint $\mathbf{x}_{k+1} = \mathbf{\Phi}\mathbf{x}_k + \mathbf{\Gamma}u_k^x$, where the influence of the exogenous disturbance on the system is neglected ($\mathbf{w}_k^d = \mathbf{0}$). In (18), $\mathbf{Q}$ is chosen to weight the squared strip displacements $w(x_i, t)$ and velocities $\dot{w}(x_i, t)$ at equidistant positions $x_i, i = 1, \ldots, \bar{m}$, along the strip length in the form

$$\mathbf{Q} = \begin{bmatrix} f_p \tilde{\mathbf{C}}^{\mathrm{T}} \tilde{\mathbf{C}} & \mathbf{0} \\ \mathbf{0} & f_v \tilde{\mathbf{C}}^{\mathrm{T}} \tilde{\mathbf{C}} \end{bmatrix},$$

with the positive weights f_p, f_v and $\tilde{\mathbf{C}} = [\hat{\mathbf{C}}^1, \ldots, \hat{\mathbf{C}}^i, \ldots, \hat{\mathbf{C}}^m]^{\mathrm{T}}$. The entries $\hat{\mathbf{C}}^i$ are given analogously to (12). The optimal feedback gain $\mathbf{K}^x$ can be computed in the form, see, e.g., [45]

$$(\mathbf{K}^x)^{\mathrm{T}} = -\big(R + \mathbf{\Gamma}^{\mathrm{T}}\mathbf{P}\mathbf{\Gamma}\big)^{-1}\big(\mathbf{\Gamma}^{\mathrm{T}}\mathbf{P}\mathbf{\Phi}\big), \tag{19}$$

where $\mathbf{P}$ solves the discrete algebraic Riccati equation

$$\mathbf{P} = \mathbf{Q} + \mathbf{\Phi}^{\mathrm{T}}\mathbf{P}\mathbf{\Phi} - \big(\mathbf{\Gamma}^{\mathrm{T}}\mathbf{P}\mathbf{\Phi}\big)^{\mathrm{T}}\big(R + \mathbf{\Gamma}^{\mathrm{T}}\mathbf{P}\mathbf{\Gamma}\big)^{-1}\big(\mathbf{\Gamma}^{\mathrm{T}}\mathbf{P}\mathbf{\Phi}\big).$$

If the pair $(\mathbf{\Phi}, \mathbf{\Gamma})$ is stabilizable and the pair $\big(\sqrt{\mathbf{Q}}, \mathbf{\Phi}\big)$ is detectable, then the system

$$\mathbf{x}_{k+1} = \Big(\mathbf{\Phi} + \mathbf{\Gamma}(\mathbf{K}^x)^{\mathrm{T}}\Big)\mathbf{x}_k, \quad \mathbf{x}_0 = \mathbf{x}(0) \tag{20}$$

is asymptotically stable. Inserting (17) into (16), we obtain the closed-loop system

$$\mathbf{x}_{k+1} = \Big(\mathbf{\Phi} + \mathbf{\Gamma}(\mathbf{K}^x)^{\mathrm{T}}\Big)\mathbf{x}_k + \Big(\mathbf{\Gamma}(\mathbf{K}^w)^{\mathrm{T}} + \mathbf{\Delta}(\omega_k)\Big)\mathbf{w}_k^d \tag{21a}$$

$$y_k = (\mathbf{C}^r)^{\mathrm{T}}\mathbf{x}_k. \tag{21b}$$

Applying the transformation [43]

$$\mathbf{z}_k = \mathbf{x}_k - \mathbf{\Pi}\mathbf{w}_k^d$$

with the yet unknown matrix $\mathbf{\Pi}$ to (21) leads to the transformed closed-loop system

$$\begin{aligned} \mathbf{z}_{k+1} =& \Big(\mathbf{\Phi} + \mathbf{\Gamma}(\mathbf{K}^x)^{\mathrm{T}}\Big)\mathbf{z}_k + \Big(\mathbf{\Delta}(\omega_k) + \mathbf{\Gamma}(\mathbf{K}^w)^{\mathrm{T}} \\ & - \mathbf{\Pi}\mathbf{\Phi}^d(\omega_k) + \Big(\mathbf{\Phi} + \mathbf{\Gamma}(\mathbf{K}^x)^{\mathrm{T}}\Big)\mathbf{\Pi}\Big)\mathbf{w}_k^d \end{aligned} \tag{22a}$$

$$y_k = (\mathbf{C}^r)^{\mathrm{T}}\mathbf{z}_k + (\mathbf{C}^r)^{\mathrm{T}}\mathbf{\Pi}\mathbf{w}_k^d \tag{22b}$$

with the new state $\mathbf{z}_k$. If

$$\mathbf{\Delta}(\omega_k) + \mathbf{\Gamma}(\mathbf{K}^w)^{\mathrm{T}} - \mathbf{\Pi}\mathbf{\Phi}^d(\omega_k) + \Big(\mathbf{\Phi} + \mathbf{\Gamma}(\mathbf{K}^x)^{\mathrm{T}}\Big)\mathbf{\Pi} = \mathbf{0} \tag{23a}$$

$$(\mathbf{C}^r)^{\mathrm{T}}\mathbf{\Pi} = \mathbf{0} \tag{23b}$$

can be solved for the unknowns $\mathbf{\Pi}$ and $\mathbf{K}^w$, (22) simplifies to the autonomous system

$$\mathbf{z}_{k+1} = \Big(\mathbf{\Phi} + \mathbf{\Gamma}(\mathbf{K}^x)^{\mathrm{T}}\Big)\mathbf{z}_k \tag{24a}$$

$$y_k = (\mathbf{C}^r)^{\mathrm{T}}\mathbf{z}_k. \tag{24b}$$

In this case, the hyperplane (manifold) $\mathbf{z}_k = \mathbf{0}$ is invariant, and since (24a) is asymptotically stable by the same line of reasoning as in (20), the output y_k asymptotically converges to zero. This shows that the closed-loop system of (16a) and (17) with $\mathbf{p}_k = \mathbf{0}$ is asymptotically stable in the new state $\mathbf{z}_k$ and that the sinusoidal disturbance w^d is asymptotically rejected in the system output y. Equation (23a) can be rewritten as a Sylvester equation [43]

$$\tilde{\mathbf{A}}\mathbf{\Pi} + \mathbf{\Pi}\tilde{\mathbf{B}} = \tilde{\mathbf{C}}, \tag{25}$$

with

$$\tilde{\mathbf{A}} = \Big(\mathbf{\Phi} + \mathbf{\Gamma}(\mathbf{K}^x)^{\mathrm{T}}\Big) \tag{26a}$$

$$\tilde{\mathbf{B}} = -\mathbf{\Phi}^d(\omega_k) \tag{26b}$$

$$\tilde{\mathbf{C}}(\mathbf{K}^w) = -\mathbf{\Delta}(\omega_k) - \mathbf{\Gamma}(\mathbf{K}^w)^{\mathrm{T}}. \tag{26c}$$

A unique solution of (25) exists if the eigenvalues of $\tilde{\mathbf{A}}$ and $-\tilde{\mathbf{B}}$ are different, see, e.g., [46]. In [36], necessary and sufficient conditions concerning the solvability of the so-called regulator equations (23b) and (25) are shown. Finally, the feedback gain $\mathbf{K}^w$ is computed as a function of ω_k. In the case of a slowly varying disturbance frequency ω, a fast real-time implementation of the controller (17) can be achieved by numerically calculating the feedback gain $\mathbf{K}^w$ for the relevant frequency range $\omega \in [\omega_l, \omega_u]$ in advance. For this purpose, an adequate discretization step $\Delta\omega$ has to be chosen and a linear interpolation between the stored feedback gains can be performed.

3.2. Observer design

Because the states of the strip $\mathbf{x}$, the disturbance $\mathbf{w}^d$, and the frequency ω cannot be measured, a state observer is designed in the form of an Extended Kalman Filter (EKF) [47] based on the measured transversal displacement at the sensor position $x = x_s$. For the observer design, $\mathbf{p}_k$ in (16a) is considered as a process noise acting on the strip dynamics. Moreover, $p_k^{w^d}$, $p_k^{\dot{w}^d}$, and p_k^{ω} are added as process noise to (16b) and (16c), respectively, and v_k represents the measurement noise in the output equation (16d). This finally yields the system

$$\bar{\mathbf{x}}_{k+1} = \bar{\mathbf{\Phi}}(\omega_k)\bar{\mathbf{x}}_k + \bar{\mathbf{\Gamma}}u_k + \bar{\mathbf{\Sigma}}\bar{\mathbf{p}}_k \tag{27a}$$

$$\bar{y}_k = \big(\bar{\mathbf{C}}^s\big)^{\mathrm{T}}\bar{\mathbf{x}}_k + v_k \tag{27b}$$

Post-print version of the article: M. Saxinger, L. Marko, A. Steinboeck, and A. Kugi, "Active rejection control for unknown harmonic disturbances of the transverse deflection of steel strips with control input, system output, sensor output, and disturbance input at different positions", *Mechatronics*, vol. 56, pp. 73–86, 2018, ISSN: 0957-4158. DOI: 10.1016/j.mechatronics.2018.10.008
The content of this post-print version is identical to the published paper but without the publisher's final layout or copy editing.

with the state vector $\bar{\mathbf{x}}_k = [\mathbf{x}_k^{\mathrm{T}}, (\mathbf{w}_k^d)^{\mathrm{T}}, \omega_k]^{\mathrm{T}}$ and

$$\bar{\mathbf{\Phi}}(\omega_k) = \begin{bmatrix} \mathbf{\Phi} & \mathbf{\Delta}(\omega_k) & \mathbf{0} \\ \mathbf{0} & \mathbf{\Phi}^d(\omega_k) & \mathbf{0} \\ \mathbf{0} & \mathbf{0} & 1 \end{bmatrix} \tag{28a}$$

$$\bar{\mathbf{\Gamma}} = \begin{bmatrix} \mathbf{\Gamma}^{\mathrm{T}} & \mathbf{0}^{\mathrm{T}} & 0 \end{bmatrix}^{\mathrm{T}} \tag{28b}$$

$$\bar{\mathbf{\Sigma}} = \begin{bmatrix} \mathbf{\Sigma} & \mathbf{0} & \mathbf{0} \\ \mathbf{0} & \mathbf{I}^{2\times 2} & \mathbf{0} \\ \mathbf{0} & \mathbf{0} & 1 \end{bmatrix} \tag{28c}$$

$$\bar{\mathbf{p}}_k = \begin{bmatrix} \mathbf{p}_k^{\mathrm{T}} & (\mathbf{p}_k^d)^{\mathrm{T}} & p_k^{\omega} \end{bmatrix}^{\mathrm{T}}, \quad (\mathbf{p}_k^d)^{\mathrm{T}} = \begin{bmatrix} p_k^{w^d} & p_k^{\dot{w}^d} \end{bmatrix} \tag{28d}$$

$$\bar{\mathbf{C}}^s = \begin{bmatrix} (\mathbf{C}^s)^{\mathrm{T}} & \mathbf{0}^{\mathrm{T}} & 0 \end{bmatrix}^{\mathrm{T}}, \quad (\mathbf{C}^s)^{\mathrm{T}} = \begin{bmatrix} \left(\hat{\mathbf{C}}^s\right)^{\mathrm{T}} & \mathbf{0}^{1\times\bar{n}} \end{bmatrix}. \tag{28e}$$

The system (27) is used as a basis for the EKF design. As usual for the EKF design, the process noise $\bar{\mathbf{p}}_k$ and the measurement noise v_k are assumed to meet the following conditions

$$\mathrm{E}(v_k) = 0 \qquad \mathrm{E}(v_k v_j) = \bar{R}\delta_{kj} \tag{29a}$$

$$\mathrm{E}(\bar{\mathbf{p}}_k) = \mathbf{0} \qquad \mathrm{E}(\bar{\mathbf{p}}_k \bar{\mathbf{p}}_j^{\mathrm{T}}) = \bar{\mathbf{Q}}_k \delta_{kj} \tag{29b}$$

$$\mathrm{E}(\bar{\mathbf{p}}_k v_j) = \mathbf{0}, \tag{29c}$$

with the Kronecker delta δ_{kj}, the covariance matrix $\bar{\mathbf{Q}}_k \geq 0$ and the variance $\bar{R} > 0$. Following [34], the EKF discrete-time (a priori) prediction equations of the state and error covariance read as

$$\hat{\bar{\mathbf{x}}}_{k+1}^- = \bar{\mathbf{\Phi}}(\hat{\omega}_k^+)\hat{\bar{\mathbf{x}}}_k^+ + \bar{\mathbf{\Gamma}} u_k \tag{30a}$$

$$\mathbf{P}_{k+1}^- = \Delta\bar{\mathbf{\Phi}}\left(\hat{\omega}_k^+, \hat{\mathbf{w}}_k^{d,+}\right)\mathbf{P}_k^+ \Delta\bar{\mathbf{\Phi}}^{\mathrm{T}}\left(\hat{\omega}_k^+, \hat{\mathbf{w}}_k^{d,+}\right) + \bar{\mathbf{\Sigma}}\bar{\mathbf{Q}}_k\bar{\mathbf{\Sigma}}^{\mathrm{T}}, \tag{30b}$$

with the state error covariance matrix $\mathbf{P}_k$. Generally, estimated values are marked with the diacritic $\hat{}$. The (a posteriori) update equations read as

$$\hat{\mathbf{L}}_k = \frac{\mathbf{P}_k^-\bar{\mathbf{C}}^s}{(\bar{\mathbf{C}}^s)^{\mathrm{T}}\mathbf{P}_k^-\bar{\mathbf{C}}^s + \bar{R}} \tag{31a}$$

$$\hat{\bar{\mathbf{x}}}_k^+ = \hat{\bar{\mathbf{x}}}_k^- + \hat{\mathbf{L}}_k\left(\bar{y}_k - (\bar{\mathbf{C}}^s)^{\mathrm{T}}\hat{\bar{\mathbf{x}}}_k^-\right) \tag{31b}$$

$$\mathbf{P}_k^+ = (\mathbf{I} - \hat{\mathbf{L}}_k(\bar{\mathbf{C}}^s)^{\mathrm{T}})\mathbf{P}_k^-. \tag{31c}$$

$\Delta\bar{\mathbf{\Phi}}\left(\hat{\omega}_k^+, \hat{\mathbf{w}}_k^{d,+}\right)$ in (30b) follows from the linearization of (27a) with respect to the state vector $\hat{\bar{\mathbf{x}}}_k^+$. Using (16e), (16g), and (28a), this gives

$$\Delta\bar{\mathbf{\Phi}}\left(\hat{\omega}_k^+, \hat{\mathbf{w}}_k^{d,+}\right) = \frac{\partial\bar{\mathbf{\Phi}}(\hat{\omega}_k^+)\hat{\bar{\mathbf{x}}}_k^+}{\partial\hat{\bar{\mathbf{x}}}_k^+} = \begin{bmatrix} \mathbf{\Phi} & \mathbf{\Delta}(\hat{\omega}_k^+) & \mathbf{\Xi}(\hat{\omega}_k^+)\hat{\mathbf{w}}_k^{d,+} \\ \mathbf{0} & \mathbf{\Phi}^d(\hat{\omega}_k^+) & \mathbf{\Xi}^d(\hat{\omega}_k^+)\hat{\mathbf{w}}_k^{d,+} \\ \mathbf{0} & \mathbf{0} & 1 \end{bmatrix}$$

with

$$\mathbf{\Xi}(\hat{\omega}_k^+) = \frac{\partial\mathbf{\Delta}(\hat{\omega}_k^+)}{\partial\hat{\omega}_k^+} = \int_0^{T_s} \exp(\mathbf{A}\tau)\left(\frac{\partial\mathbf{G}}{\partial\omega}\right)(\hat{\omega}_k^+)\exp\left(\mathbf{A}^d(\hat{\omega}_k^+)(T_s-\tau)\right)\mathrm{d}\tau + \int_0^{T_s} \exp(\mathbf{A}\tau)\mathbf{G}(\hat{\omega}_k^+)\exp\left(\mathbf{A}^d(\hat{\omega}_k^+)(T_s-\tau)\right)\left(\frac{\partial\mathbf{A}^d}{\partial\omega}\right)(\hat{\omega}_k^+)(T_s-\tau)\mathrm{d}\tau \tag{32a}$$

$$\mathbf{\Xi}^d(\hat{\omega}_k^+) = \frac{\partial\mathbf{\Phi}^d(\hat{\omega}_k^+)}{\partial\hat{\omega}_k^+} = \exp\left(\mathbf{A}^d(\hat{\omega}_k^+)T_s\right)\left(\frac{\partial\mathbf{A}^d}{\partial\omega}\right)(\hat{\omega}_k^+)T_s. \tag{32b}$$

A suitable choice of the initial conditions $\hat{\bar{\mathbf{x}}}_0^-$ and $\mathbf{P}_0^-$ completes the design of the EKF.

The estimated transversal displacement of the strip at the positions $x = x_s$ of the displacement sensor, $x = x_r$ of the system output (gas wiping dies), $x = x_m$ of the electromagnetic actuator, and at the laser distance sensor positions $x = x_{lsr\,i}$, $i = 1, \ldots, 10$ (only used for validation purpose) read as

$$\hat{y}_k = \hat{w}_k^s = (\bar{\mathbf{C}}^s)^{\mathrm{T}}\hat{\bar{\mathbf{x}}}_k, \quad \hat{w}_k^r = (\bar{\mathbf{C}}^r)^{\mathrm{T}}\hat{\bar{\mathbf{x}}}_k, \quad \hat{w}_k^m = (\bar{\mathbf{C}}^m)^{\mathrm{T}}\hat{\bar{\mathbf{x}}}_k$$

and

$$\hat{w}_k^{lsr\,i} = (\bar{\mathbf{C}}^{lsr\,i})^{\mathrm{T}}\hat{\bar{\mathbf{x}}}_k, \qquad i \in [1, \ldots, 10].$$

The structure of all $\bar{\mathbf{C}}^\kappa$ with $\kappa \in \{r, m, lsr\,i\}$ is similar to (28e). Finally, if the control law (17) is combined with the EKF (30), (31), we get

$$u_k = \mathbf{K}(\hat{\omega}_{k+1}^-)\hat{\bar{\mathbf{x}}}_{k+1}^- = \begin{bmatrix} (\mathbf{K}^x)^{\mathrm{T}} & \left(\mathbf{K}^w(\hat{\omega}_{k+1}^-)\right)^{\mathrm{T}} & 0 \end{bmatrix}\hat{\bar{\mathbf{x}}}_{k+1}^-$$

with $\mathbf{K}^x$ from (19) and $\mathbf{K}^w(\hat{\omega}_{k+1}^-)$ as the solution of the regulator equations (23b) and (25) for the frequency $\hat{\omega}_{k+1}^-$. Here, $\hat{\bar{\mathbf{x}}}_{k+1}^-$ is used instead of $\hat{\bar{\mathbf{x}}}_k^+$ to compensate for the computational time delay.

4. Experimental setup

In the following, we will give a more detailed description of the components of the experimental test rig outlined in Fig. 3. Figure 4 shows a photo of the setup. An overview of the used components is given in Table 1. The steel strips which can be used in the experiment have lengths L between 1.9 m and 2.1 m, their thicknesses h range from 0.5 mm to 1.5 mm and their width b is 150 mm. A dSPACE *MicroLabBox* control system platform is used as real-time hardware to record the measurement signals and to accommodate the observer and controller implementation.

Post-print version of the article: M. Saxinger, L. Marko, A. Steinboeck, and A. Kugi, "Active rejection control for unknown harmonic disturbances of the transverse deflection of steel strips with control input, system output, sensor output, and disturbance input at different positions", *Mechatronics*, vol. 56, pp. 73–86, 2018, ISSN: 0957-4158. DOI: 10.1016/j.mechatronics.2018.10.008
The content of this post-print version is identical to the published paper but without the publisher's final layout or copy editing.

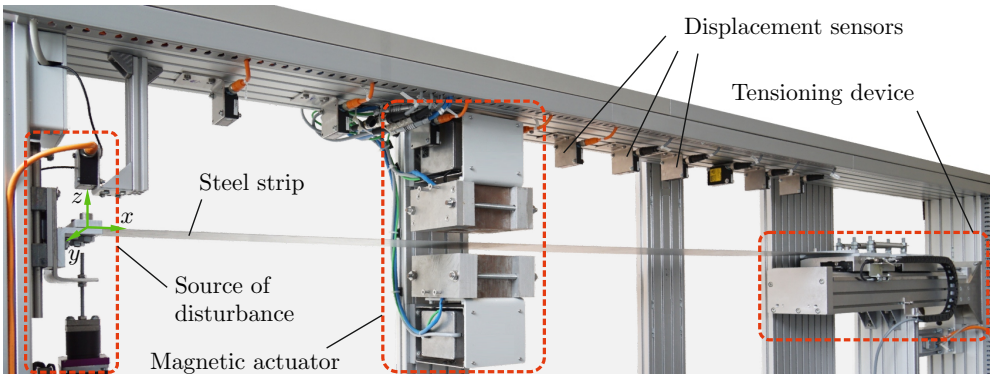

Figure 4: Experimental test rig with a clamped steel strip.

component	product, type (specification)
tensioning device	
linear axis (slides)	FESTO, *EGC-185-700-BS*
parallel kit	FESTO, *EAMM-U*
gear unit	FESTO, *EMGA-SAS*
servo drive	FESTO, *EMME-AS*
force sensor	INELTA, *KMM20-5kN*
spring	GUTEKUNST, *RZ-162U-43I* (three springs in parallel)
source of disturbance	
electromechanical cylinder	GUNDA-GMBH, *Colibri-L KE 23K10*
linear guide	IGUS, *DryLin W: WS-10-120* IGUS, *WW-10-120-10*
laser displacement sensors	WELOTEC, *OWLE 5060 S1*
magnets	
current controller	MAXON, *ESCON 50/5*
air gap δ^{cc}	(50 mm)
number of windings	(280)
dimension of core in x-direction	(100 mm)
real-time system	DSPACE, *MicroLabBox*

Table 1: Components of the experimental test rig.

4.1. Tensioning device

The tensioning device consists of a non-driven (passive) slide which is connected to a driven (active) slide by means of three springs in parallel. One end of the strip is clamped in the passive slide. At the other end, the strip is connected to a slide, which can move along the direction z (transverse strip direction). The force N_{xx} in the strip is controlled by means of the elongation of calibrated springs between the active and the passive slide. For calibrating the springs, a force sensor was used. Compared to the strip, the spring has a low stiffness, which allows an accurate adjustment of the desired tensile load N_{xx} by controlling the position of the active slide.

4.2. Displacement sensors

The experimental test rig is equipped with ten laser triangulation sensors referred to as $\mathrm{lsr}\,1, \ldots, \mathrm{lsr}\,10$ in Fig. 3. They are located at the equidistant positions $x_{lsr\,1}, \ldots, x_{lsr\,10}$ and they are used for measuring the strip shape during the experiments. The sensors are only used for validation purposes. Only one of them is utilized for control, i.e., the sensor at the position x_s (sensor output).

4.3. Source of disturbance

At the boundary $x = 0$, the transverse displacement of the strip $w^d(t) = w(0,t)$ is prescribed by a disturbance actuator. This motion is considered as an external disturbance in the form of a sinusoidal signal with various frequencies and amplitudes. The slope of the strip is always zero at this point.

Post-print version of the article: M. Saxinger, L. Marko, A. Steinboeck, and A. Kugi, "Active rejection control for unknown harmonic disturbances of the transverse deflection of steel strips with control input, system output, sensor output, and disturbance input at different positions", *Mechatronics*, vol. 56, pp. 73–86, 2018, ISSN: 0957-4158. DOI: 10.1016/j.mechatronics.2018.10.008
The content of this post-print version is identical to the published paper but without the publisher's final layout or copy editing.

4.4. Magnetic actuator

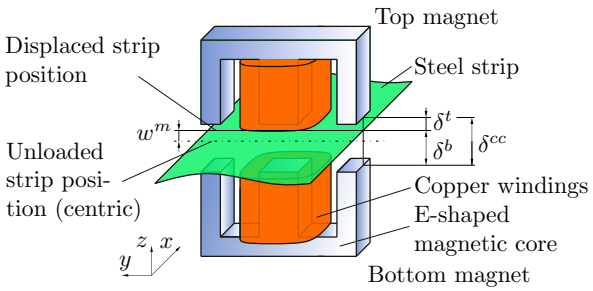

Figure 5: Magnetic actuator.

Figure 5 outlines the custom-made magnetic actuator. The electromagnetic force F^m is always attractive, which is why a pair of magnets is necessary to apply forces in both directions (positive and negative z-direction) to the strip. For the magnets, a compact design yielding high electromagnetic forces without saturating the magnetic core was chosen. To minimize eddy currents, the magnetic core is laminated, see also [7, 48, 49, 19]. However, saturation of the thin steel strip itself cannot be prevented with reasonable effort, see [7]. Figure 6 shows the measured quasi-static electromagnetic force $F^m = f\big(I^t, I^b, w^m\big)$ as a function of the transversal strip displacement w^m and the currents I^t and I^b supplied to the top and bottom magnet, respectively. This measurement was performed in a special setup for characterizing the magnets which, in contrast to the experimental test rig of Fig. 4, was equipped with force sensors. Based on the transversal strip displacement w^m, the air gap between the strip and the top and bottom magnet read as

$$\delta^t = \frac{\delta^{cc}}{2} - w^m \quad \text{and} \quad \delta^b = \frac{\delta^{cc}}{2} + w^m,$$

respectively, with the air gap between the top and bottom magnet δ^{cc}. Since the electromagnetic force F^m acting on the strip cannot be directly measured, neither in the experimental test rig of Fig. 4 nor in the real plant according to Fig. 1, a feedforward controller which inverts the current-force characteristics depicted in Fig. 6 is employed. In a discrete-time setting, the electromagnetic force $F_k^{m,ref}$ at the sampling time t_k for the (estimated) displacement $\hat{w}_k^m$ is realized by subordinate PI current controllers with the reference values

$$I_k^{t,ref} = \begin{cases} f^{-1}\left(\hat{w}_k^m, F_k^{m,ref}\right) & \text{for } F_k^{m,ref} \geq 0 \\ 0 & \text{else} \end{cases} \tag{33a}$$

$$I_k^{b,ref} = \begin{cases} 0 & \text{for } F_k^{m,ref} \geq 0 \\ f^{-1}\left(\hat{w}_k^m, F_k^{m,ref}\right) & \text{else.} \end{cases} \tag{33b}$$

Note that this feedforward approach is only feasible for quasi-static operation where eddy currents are negligible. According to Faraday's law of induction, eddy currents are caused by the rate of change in the magnetic field and therefore significantly increase with the frequency of the disturbance. Moreover, the force dynamics of the magnetic actuator is negatively influenced by eddy currents, see [7].

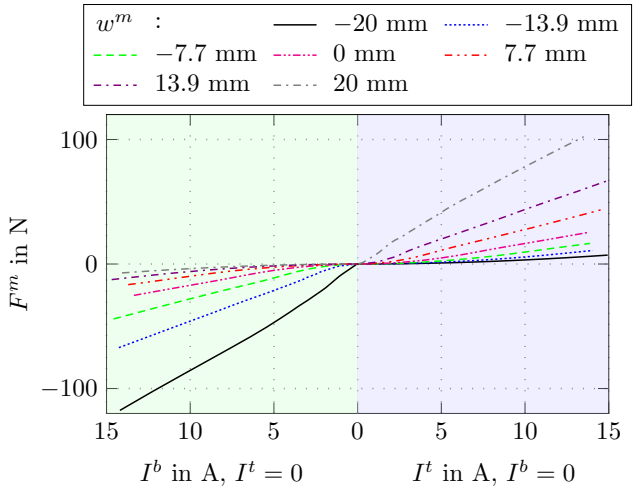

Figure 6: Measured electromagnetic force acting on the strip depending on the transversal strip displacement w^m and the currents I^t and I^b supplied to the top and bottom magnet.

5. Experimental results

A block diagram of the control concept is shown in Fig. 7. Here, the green domain consisting of the subordinate PI current controllers with the reference values according to (33) comprises the discrete-time feedforward control for the electromagnetic force described in Section 4. The blue domain consisting of the LQR, the disturbance feedforward controller from Section 3.1, and the observer from Section 3.2 comprises the discrete-time vibration control strategy described in Section 3. Except the separate PI current controllers, which all have sampling times of $T_s^{PI} = 1/(53.6 \cdot 10^3)\,\text{s}$, the control concept is implemented on a real-time hardware with the sampling time $T_s = 1 \cdot 10^{-3}\,\text{s}$. The parameters of the PI current controllers were manually tuned and configured with the MAXON ESCON STUDIO in order to achieve a good control performance. Fig. 8 shows the reference I^{ref} and the measured currents I^t and I^b of the PI current controllers for the top and bottom magnet, where an approximately sinusoidal force with $\max\big(|F^{m,ref}|\big) \approx 2\,\text{N}$ is applied. The signals in Fig. 8 constitute a worst case scenario with the disturbance frequency $f^d = 9\,\text{Hz}$. Nevertheless, the measurements show that the controlled currents accurately coincide with the desired reference trajectory I^{ref}. Table 2 contains all the parameters used in the mathematical model of Section 2. Except for the damping parameters μ and λ, which were determined in a measurement campaign, all other parameters are assigned their nominal values. Figure 9 shows the measured and simulated strip displacement w^m at the position x_m. Because w^m cannot

Post-print version of the article: M. Saxinger, L. Marko, A. Steinboeck, and A. Kugi, "Active rejection control for unknown harmonic disturbances of the transverse deflection of steel strips with control input, system output, sensor output, and disturbance input at different positions", *Mechatronics*, vol. 56, pp. 73–86, 2018, ISSN: 0957-4158. DOI: 10.1016/j.mechatronics.2018.10.008
The content of this post-print version is identical to the published paper but without the publisher's final layout or copy editing.

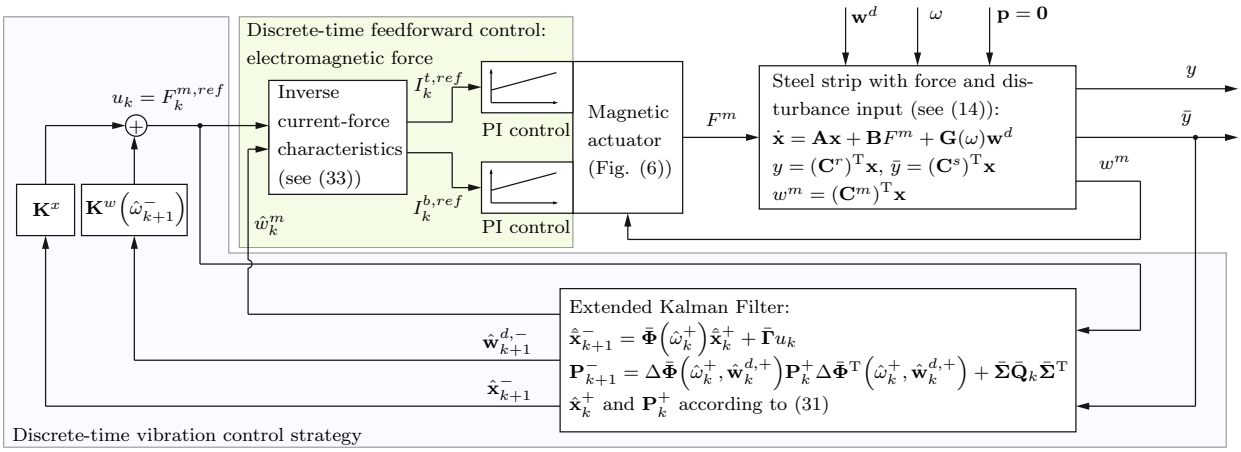

Figure 7: Block diagram of the overall control system.

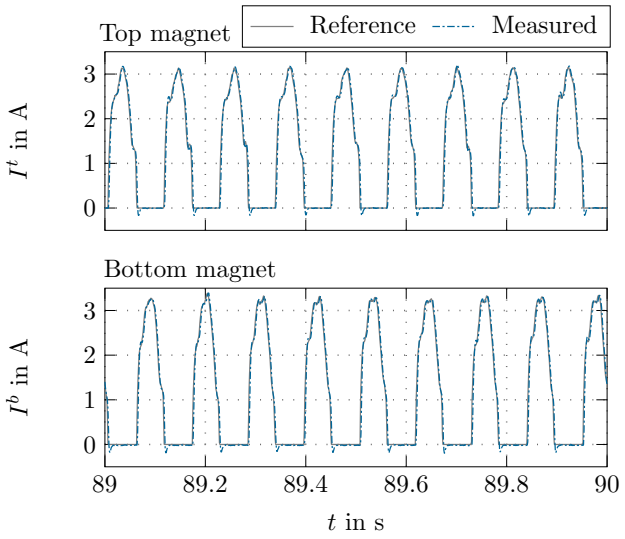

Figure 8: Measurements showing the performance of the PI current controllers. Settings in the MAXON ESCON STUDIO: proportional gain $K_p = 11\,831$; integral time constant $T_n = 2442\,\mu s$; the supply voltage was 48 V.

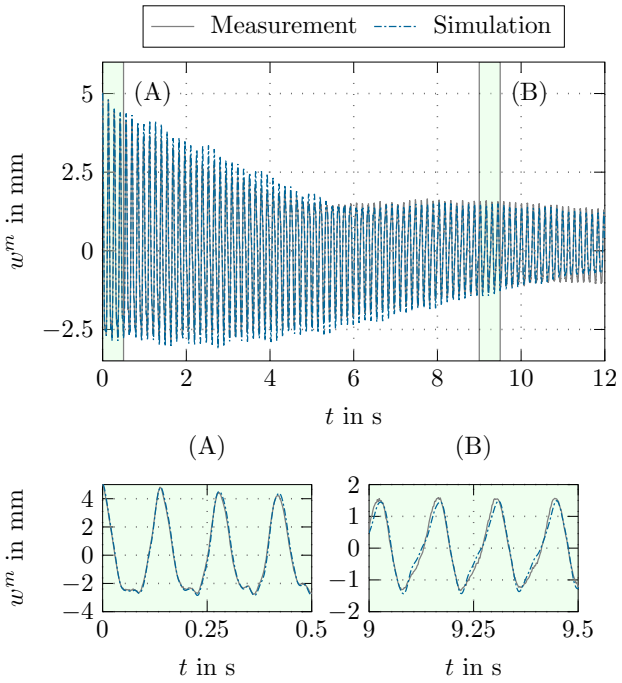

Figure 9: Strip displacement w^m at the position x_m for an initial displacement $w^m(0) = 5\,\text{mm}$.

be directly measured, see Fig. 3, it is approximated by the linear interpolation of the measurements $w^{lsr\,3}$ and $w^{lsr\,4}$. The results show that the mathematical model accurately captures the dynamic behavior of the system.

The tuning parameters for the optimal state controller of Section 3.1 are given in Table 3. These parameters were determined by in-situ manual tuning. The parametrization of the EKF according to Section 3.2 is given in Table 4. The variance $\bar{R}$ of the measurement noise of the displacement sensor at the position $x = x_s$ can be easily obtained from measurement results. The covariance matrix $\bar{\mathbf{Q}}_k \geq 0$ of the process noise, see (30b), is chosen in the form

$$\bar{\mathbf{Q}}_k = \operatorname{diag}\left(\underbrace{\bar{Q}^p, \ldots, \bar{Q}^p}_{n-1}, \bar{Q}_k^{w^d}, \bar{Q}_k^{\dot{w}^d}, \bar{Q}^{\omega}\right)$$

with positive weighting parameters $\bar{Q}^p$, $\bar{Q}_k^{w^d}$, $\bar{Q}_k^{\dot{w}^d}$, and $\bar{Q}^{\omega}$. While $\bar{Q}^p$ and $\bar{Q}^{\omega}$ are chosen constant, it turned out to be beneficial for the performance to make $\bar{Q}_k^{w^d}$ and $\bar{Q}_k^{\dot{w}^d}$ depend on the (slowly varying) estimated frequency $\hat{\omega}_k^-$.

Post-print version of the article: M. Saxinger, L. Marko, A. Steinboeck, and A. Kugi, "Active rejection control for unknown harmonic disturbances of the transverse deflection of steel strips with control input, system output, sensor output, and disturbance input at different positions", *Mechatronics*, vol. 56, pp. 73–86, 2018, ISSN: 0957-4158. DOI: 10.1016/j.mechatronics.2018.10.008
The content of this post-print version is identical to the published paper but without the publisher's final layout or copy editing.

Effectively, the affine relation

$$\bar{Q}_k^{w^d} = \bar{Q}_k^{w^d,2\pi} + \left(\bar{Q}_k^{w^d,18\pi} - \bar{Q}_k^{w^d,2\pi}\right)\frac{\hat{\omega}_k^- - 2\pi}{16\pi} \quad (34a)$$

$$\bar{Q}_k^{\dot{w}^d} = \bar{Q}_k^{\dot{w}^d,2\pi} + \left(\bar{Q}_k^{\dot{w}^d,18\pi} - \bar{Q}_k^{\dot{w}^d,2\pi}\right)\frac{\hat{\omega}_k^- - 2\pi}{16\pi} \quad (34b)$$

is used for the relevant frequency range $2\pi\,\mathrm{rad/s} \leq \omega \leq 18\pi\,\mathrm{rad/s}$. The idea of an online adaption of the covariances can be found at different places in literature, see, e.g., [47]. A validation of the EKF was carried out at the experimental test rig by comparing the observed transversal strip displacements with the displacements measured by the laser sensors according to Fig. 10. For this experiment, the frequency $f^d = \omega/(2\pi)$ was varied. Figure 10 reveals a good accordance of the estimated frequency $\hat{f}^d$ with the time-varying disturbance frequency f^d. A slightly increased estimation error of the disturbance frequency in the vicinity of 110 s is obtained. Here, the undamped natural strip vibrations are dominant compared to the vibrations caused by the disturbance actuator. Therefore, it is hard for the estimator to accurately track the real disturbance frequency f^d. The results for the two arbitrarily chosen sensors lsr 2 and lsr 7 are also shown in Fig. 10. The other sensors yield similar results. In particular, the bottom part of Fig. 10 demonstrates the good performance of the EKF.

A typical vibration of the strip for a harmonic disturbance $w^d(t)$ (blue line) with the frequency $f^d = 4\,\mathrm{Hz}$ and 1 mm amplitude, where the controller is off, is shown in Fig. 11. Figure 12 presents the transversal strip displacement at the positions of the laser sensors for different disturbance frequencies f^d and active control. The blue line corresponds to the disturbance input $w^d(t)$, the red line is the only sensor signal used in the control concept, and the green line is the system output, where the vibrations have to be suppressed. As can be seen, the controller does a good job in rejecting the oscillations in the system output y.

The frequency spectra of the displacement measurements are shown in Fig. 13, without control on the left hand side and with active control on the right hand side. Moreover, the peak values $\max\left(|F^{m,ref}|\right)$ of the electromagnetic force $F^{m,ref}$ (control input) are also displayed in the subplots. The natural frequencies of the strip are indicated as dashed ochre-brown lines. The disturbance is not a strictly sinusoidal signal, see Figs. 11 and 12. However, the higher harmonics are small and can be neglected. Clearly, the theory presented in this paper can be extended to also reject higher harmonics.

Despite the assumption of a constant disturbance frequency f^d used in the observer and controller design, the concept was also tested for slowly varying frequencies. The corresponding results are shown in Fig. 14. The range of f^d was chosen to include the first natural frequency of the strip. In Fig. 14, the frequency of the disturbance equals the first natural frequency at approximately 65 s and 110 s. If the control is inactive, high amplitudes of the system output y do occur at these times (resonance). The vibrations are reduced drastically in the case of active control. In contrast to the frequency estimate $\hat{f}^d$ for an inactive control in Fig. 10, where the estimation error is slightly increased in the vicinity of the first natural frequency (110 s), the frequency estimate $\hat{f}^d$ follows the time-varying disturbance frequency f^d quite well in the case of active control, see Fig. 14. Here, the vibrations due to the first natural frequency of the strip are reduced by the LQR feedback controller. The frequency of the disturbance passes a transmission zero of the plant at about 81 s and 95 s, see Fig. 14, which results in small amplitudes even for inactive control. However, the amplitudes are further reduced by the controller. During the whole experiment, the required electromagnetic force $F^{m,ref}$ does not exceed $\pm 4\,\mathrm{N}$. The picture details (A)-(C) highlight the performance of the proposed control concept. The vibration at the system output y is clearly reduced, even if the disturbance frequency is changing.

Post-print version of the article: M. Saxinger, L. Marko, A. Steinboeck, and A. Kugi, "Active rejection control for unknown harmonic disturbances of the transverse deflection of steel strips with control input, system output, sensor output, and disturbance input at different positions", *Mechatronics*, vol. 56, pp. 73–86, 2018, ISSN: 0957-4158. DOI: 10.1016/j.mechatronics.2018.10.008
The content of this post-print version is identical to the published paper but without the publisher's final layout or copy editing.

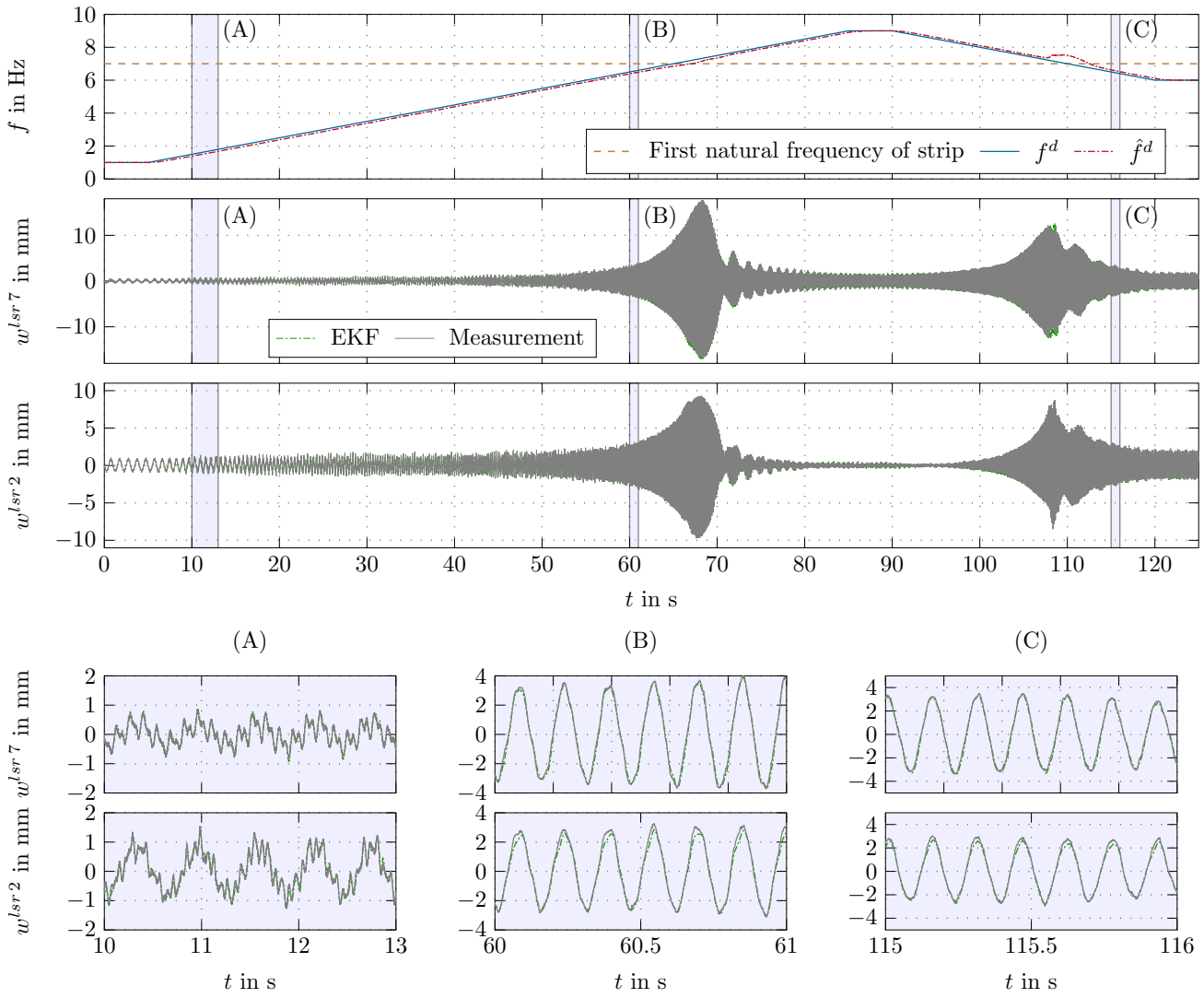

Figure 10: Validation of the EKF.

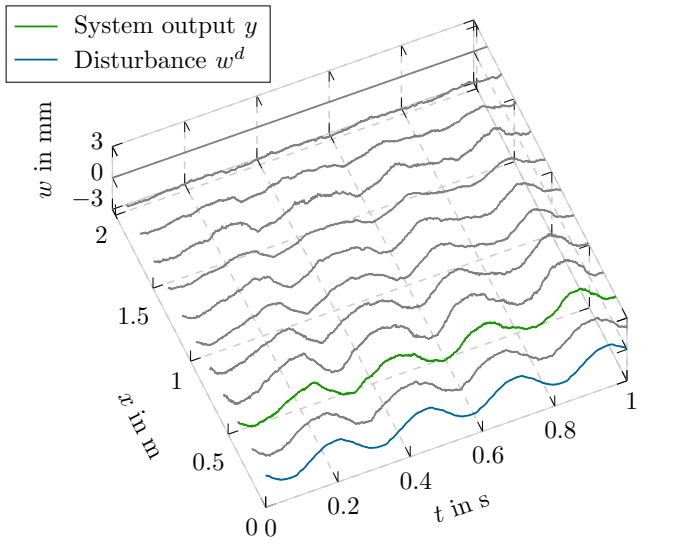

Figure 11: Measured strip displacement caused by a disturbance w^d with the frequency $f^d = 4\,\text{Hz}$ and the amplitude 1 mm without control

6. Conclusions and outlook

This article dealt with rejection control of an unknown sinusoidal disturbance at an arbitrarily chosen position of a vibrating steel strip. A custom-made electromagnetic actuator is used to apply the control force to the metal strip. A single displacement sensor is necessary for the proposed control method.

The main findings of this study are as follows:

- An algorithm for the rejection of an unknown sinusoidal disturbance was developed for a non-collocated sensor-actuator setup and validated based on an experimental test rig.
- The control and observer configuration works well.
- The positions of disturbance, sensor, actuator, and system output can be different and arbitrarily chosen.

Post-print version of the article: M. Saxinger, L. Marko, A. Steinboeck, and A. Kugi, "Active rejection control for unknown harmonic disturbances of the transverse deflection of steel strips with control input, system output, sensor output, and disturbance input at different positions", *Mechatronics*, vol. 56, pp. 73–86, 2018, ISSN: 0957-4158. DOI: 10.1016/j.mechatronics.2018.10.008
The content of this post-print version is identical to the published paper but without the publisher's final layout or copy editing.

specification	parameter	value, unit
strip length	L	2.04 m
strip width	b	150 mm
strip thickness	h	0.76 mm
density	ρ	7850 kg/m^3
Young's modulus	E	$2.1 \cdot 10^{11}$ N/m^2
tensile load	N_{xx}	687 N
viscous damping factor	μ	0.232/s
material damping factor	λ	$4.67 \cdot 10^{-6}$ s
position of magnet	x_m	0.649 m
dimension of magnet	Δx_m	0.1 m
position of sensor	x_s	0.927 m
position of output	x_r	0.371 m
amplitude of disturbance	d	1 mm
number of finite elements	n	9

Table 2: Parameters of the mathematical model.

specification	parameter	value, unit
weight for position	f_p	$5\,(1/\mathrm{m})^2$
weight for velocities	f_v	$0.06\,(\mathrm{s/m})^2$
weight for the input	R	$0.005\,(1/\mathrm{N})^2$
weighting points	$\bar{m}$	23

Table 3: Parameters used for the LQR.

specification	parameter	value, unit
sensor noise	$\bar{R}$	$2.25 \cdot 10^{-8}$ m^2
process noise strip	$\bar{Q}^p$	$10\,(\mathrm{N/m})^2$
process noise disturbance:		
position (lower limit)	$\bar{Q}^{w^d,2\pi}$	$2.25 \cdot 10^{-12}$ m^2
position (upper limit)	$\bar{Q}^{w^d,18\pi}$	$2.25 \cdot 10^{-10}$ m^2
velocity (lower limit)	$\bar{Q}^{\dot{w}^d,2\pi}$	$4.4 \cdot 10^{-9}\,(\mathrm{m/s})^2$
velocity (upper limit)	$\bar{Q}^{\dot{w}^d,18\pi}$	$4.4 \cdot 10^{-7}\,(\mathrm{m/s})^2$
frequency	$\bar{Q}^{\omega}$	$2 \cdot 10^{-4}\,(\mathrm{rad/s})^2$

Table 4: Parameters used for the EKF.

- The experiment was inspired by the conditions observed in hot-dip galvanizing lines.
- A calibrated quasi-static relation between electromagnetic force, the transversal strip displacement, and the currents of both coils (top and bottom magnet) was used to apply forces in both directions to the strip. The required currents have been realized by subordinate current PI controllers.
- The proposed control method works well without applying a force sensor for measuring the magnetic force or an extra distance sensor for measuring the strip displacement at the position of the magnets.
- The observer and controller configuration is robust against process noise and deviations from an ideal sinusoidal disturbance.

Stimulated by the good control performance observed in the experimental rig, the implementation of the developed control method in an industrial hot-dip galvanizing line is intended for the near future.

7. Acknowledgments

The financial support by the Austrian Federal Ministry for Digital and Economic Affairs and the National Foundation for Research, Technology and Development, and voestalpine Stahl GmbH is gratefully acknowledged.

[1] Y.-H. Kweon, H.-D. Kim, Study on the wiping gas jet in continuous galvanizing line, Journal of Thermal Science 20 (3) (2011) 242–247.
[2] M. Takeda, M. Watanabe, Self-excited vibration of a plate supported by air pressure in a floating conveying machine, American Society of Mechanical Engineers, Pressure Vessels and Piping Division (Publication) PVP 4 (2017) 1–10.
[3] M. Saxinger, A. Steinboeck, M. Baumgart, P. Kerschbaummayr, A. Kugi, Influence of air cooling jets on the steady-state shape of strips in hot dip galvanizing lines, IFAC-PapersOnLine 28 (17) (2015) 143–148.
[4] S. Hui, H. Zhang, J. Ma, P. Xu, One-third sub-harmonic resonance analysis for the up-going strip emerging from the zinc pot, Key Engineering Materials 693 (2016) 1247–1254.
[5] J. Li, Y.-H. Yan, X.-H. Guo, Y.-Q. Wang, Research on vibration control method of steel strip for a continuous hot-dip galvanizing line, ISIJ International 52 (6) (2012) 1072–1079.
[6] ANDRITZ Metals, Hot dip galvanizing line no. 5, voestalpine AG, Austria, https://www.andritz.com/resource/blob/77380/80a71edeed68605d04572dcee6be66b5/me-hotdipgalvanizinglineno5-brochure-en-data.pdf, accessed: 2018-08-24 (2013).
[7] L. Marko, M. Saxinger, A. Steinboeck, A. Kugi, Magnetic actuator design for strip stabilizers in hot dip galvanizing lines, Accepted for presentation at the IEEE Industry Applications Society Annual Meeting (2018).
[8] N. Guelton, C. Lopès, H. Sordini, Cross coating weight control by electromagnetic strip stabilization at the continuous galvanizing line of arcelormittal florange, Metallurgical and Materials Transactions B 47 (4) (2016) 2666–2680.
[9] M. Shigeki, I. Atsushi, S. Hideaki, N. Kazuhisa, K. Keiichi, Study on shape control and vibration absorber of strip in steel process line, Mitsubishi Heavy Industries Ltd. Technical Review 32 (3) (1995) 5–8.

Post-print version of the article: M. Saxinger, L. Marko, A. Steinboeck, and A. Kugi, "Active rejection control for unknown harmonic disturbances of the transverse deflection of steel strips with control input, system output, sensor output, and disturbance input at different positions", *Mechatronics*, vol. 56, pp. 73–86, 2018, ISSN: 0957-4158. DOI: 10.1016/j.mechatronics.2018.10.008
The content of this post-print version is identical to the published paper but without the publisher's final layout or copy editing.

[10] W. Jung, Y. Jang, S. Lim, S. Won, Active vibration and flatness control of a strip in a continuous galvanizing line using positive position feedback control, ISIJ International 53 (5) (2013) 854–865.

[11] J.-Y. Choi, K.-S. Hong, K.-J. Yang, Exponential stabilization of an axially moving tensioned strip by passive damping and boundary control, Journal of Vibration and Control 10 (5) (2004) 661–682.

[12] A. Preumont, Vibration Control of Active Structures: An Introduction, Solid Mechanics and Its Applications, Springer, Netherlands, 2011.

[13] C. Vasques, J. Dias Rodrigues, Active vibration control of smart piezoelectric beams: Comparison of classical and optimal feedback control strategies, Computers and Structures 84 (22-23) (2006) 1402–1414.

[14] D. L. Trumper, M.-C. Weng, R. J. Ritter, Magnetic suspension and vibration control of beams for non-contact processing, IEEE Conference on Control Applications - Proceedings 1 (1999) 551–557.

[15] E. Omidi, S. Mahmoodi, J. Shepard, W.S., Multi positive feedback control method for active vibration suppression in flexible structures, Mechatronics 33 (2016) 23–33.

[16] J. Cannon, R.H., D. Rosenthal, Experiments in control of flexible structures with noncolocated sensors and actuators, Journal of Guidance, Control, and Dynamics 7 (5) (1984) 546–553.

[17] Q. Zhang, S. Shelley, R. Allemang, Active damping design of flexible structures based on SISO and SIMO noncollocated sensor-actuator velocity feedback, Journal of Dynamic Systems, Measurement and Control, Transactions of the ASME 113 (2) (1991) 259–266.

[18] B. Yang, J. Mote, C.D., Active vibration control of the axially moving string in the s domain, Journal of Applied Mechanics, Transactions ASME 58 (1) (1991) 189–196.

[19] B. Gospodarič, D. Vončina, B. Bučar, Active electromagnetic damping of laterally vibrating ferromagnetic cantilever beam, Mechatronics 17 (6) (2007) 291 – 298.

[20] S. Skogestad, I. Postlethwaite, Multivariable Feedback Control: Analysis and Design, Wiley, Chichester, 2005.

[21] L. Iorga, H. Baruh, I. Ursu, A review of H_∞ robust control of piezoelectric smart structures, Applied Mechanics Reviews 61 (1-6) (2008) 0408021–04080215.

[22] Z.-C. Qiu, B. Ma, Adaptive resonant vibration control of a piezoelectric flexible plate implementing filtered-X LMS algorithm, International Journal of Acoustics and Vibrations 19 (4) (2014) 224–239.

[23] J.-E. Oh, Active vibration control of flexible cantilever beam using piezo actuator and filtered-X LMS algorithm, KSME International Journal 12 (4) (1998) 665–671.

[24] L. Sievers, A. von Flotow, Comparison and extensions of control methods for narrow-band disturbance rejection, IEEE Transactions on Signal Processing 40 (10) (1992) 2377–2391.

[25] G. De Nicolao, F. Lorito, S. Strada, On 'Comparison and extensions of control methods for narrow-band disturbance rejection', IEEE Transactions on Speech and Audio Processing 2 (3) (1994) 459–461.

[26] M. Bodson, Rejection of periodic disturbances of unknown and time-varying frequency, International Journal of Adaptive Control and Signal Processing 19 (2-3) (2005) 67–88.

[27] H. Shim, H. Kim, C. Chung, Design and experiment of add-on track following controller for optical disc drives based on robust output regulation, Proceedings of the American Control Conference 2 (2004) 1829–1835.

[28] W. Kim, H. Kim, C. C. Chung, M. Tomizuka, Adaptive output regulation for the rejection of a periodic disturbance with an unknown frequency, IEEE Transactions on Control Systems Technology 19 (5) (2011) 1296–1304.

[29] H. Kim, H. Shim, N. H. Jo, Adaptive add-on output regulator for rejection of sinusoidal disturbances and application to optical disc drives, IEEE Transactions on Industrial Electronics 61 (10) (2014) 5490–5499.

[30] M. Ficocelli, F. Amara, Adaptive regulation of MIMO linear systems against unknown sinusoidal exogenous inputs, International Journal of Adaptive Control and Signal Processing 23 (6) (2009) 581–603.

[31] G. Obregón-Pulido, B. Castillo-Toledo, A. Loukianov, A structurally stable globally adaptive internal model regulator for MIMO linear systems, IEEE Transactions on Automatic Control 56 (1) (2011) 160–165.

[32] W.-H. Chen, Disturbance observer based control for nonlinear systems, IEEE/ASME Transactions on Mechatronics 9 (4) (2004) 706–710.

[33] J. Deutscher, Output regulation for linear distributed-parameter systems using finite-dimensional dual observers, Automatica 47 (11) (2011) 2468–2473.

[34] D. Simon, Optimal State Estimation: Kalman, H Infinity, and Nonlinear Approaches, John Wiley & Sons, New Jersey, 2006.

[35] A. Isidori, L. Marconi, A. Serrani, Robust Autonomous Guidance: An Internal Model Approach, Advances in Industrial Control, Springer, London, 2003.

[36] C. Byrnes, A. Isidori, Output regulation for nonlinear systems: An overview, International Journal of Robust and Nonlinear Control 10 (5) (2000) 323–337.

[37] H. Knobloch, A. Isidori, D. Flockerzi, Topics in control theory, DMV Seminar, Birkhäuser Verlag, Basel, 1993.

[38] M. Saxinger, A. Steinboeck, M. Baumgart, A. Kugi, Dynamical model of axially moving steel strips, IFAC-PapersOnLine 49 (20) (2016) 190–195.

[39] M. Saxinger, A. Steinboeck, L. Marko, M. Baumgart, A. Kugi, Nonlinear dynamical model of an axially moving steel strip in a surface coating plant (in german), at-automatisierungstechnik 65 (8) (2017) 546–560.

[40] R. M. Bozorth, Ferromagnetism, Wiley Interscience, IEEE Press, New Jersey, 1993.

[41] J. Reddy, Theory and Analysis of Elastic Plates and Shells, 2nd Edition, CRC Press, Boca Raton, London, New York, 2007.

[42] M. Liu, D. Gorman, Formulation of Rayleigh damping and its extensions, Computers & Structures 57 (2) (1995) 277–285.

[43] T. Rittenschober, K. Schlacher, Observer-based self sensing actuation of piezoelastic structures for robust vibration control, Automatica 48 (6) (2012) 1123–1131.

[44] A. Isidori, Nonlinear Control Systems, Communications and Control Engineering, Springer, London, 1995.

[45] K. Åström, B. Wittenmark, Computer-controlled Systems: Theory and Design, 3rd Edition, Prentice Hall, Upper Saddle River, New Jersey, 1997.

[46] R. H. Bartels, G. W. Stewart, Solution of the matrix equation AX + XB = C [f4], Communications of the ACM 15 (9) (1972) 820–826.

[47] M. Boutayeb, D. Aubry, A strong tracking extended Kalman observer for nonlinear discrete-time systems, IEEE Transactions on Automatic Control 44 (8) (1999) 1550–1556.

[48] E. Maslen, G. Schweitzer, H. Bleuler, M. Cole, P. Keogh, R. Larsonneur, R. Nordmann, Y. Okada, A. Traxler, Magnetic Bearings: Theory, Design, and Application to Rotating Machinery, Springer, Berlin Heidelberg, 2009.

[49] E. Kallenbach, R. Eick, P. Quendt, T. Ströhla, K. Feindt, M. Kallenbach, Elektromagnete: Grundlagen, Berechnung, Entwurf und Anwendung, Vieweg + Teubner, Wiesbaden, 2008.

Post-print version of the article: M. Saxinger, L. Marko, A. Steinboeck, and A. Kugi, "Active rejection control for unknown harmonic disturbances of the transverse deflection of steel strips with control input, system output, sensor output, and disturbance input at different positions", *Mechatronics*, vol. 56, pp. 73–86, 2018, ISSN: 0957-4158. DOI: 10.1016/j.mechatronics.2018.10.008
The content of this post-print version is identical to the published paper but without the publisher's final layout or copy editing.

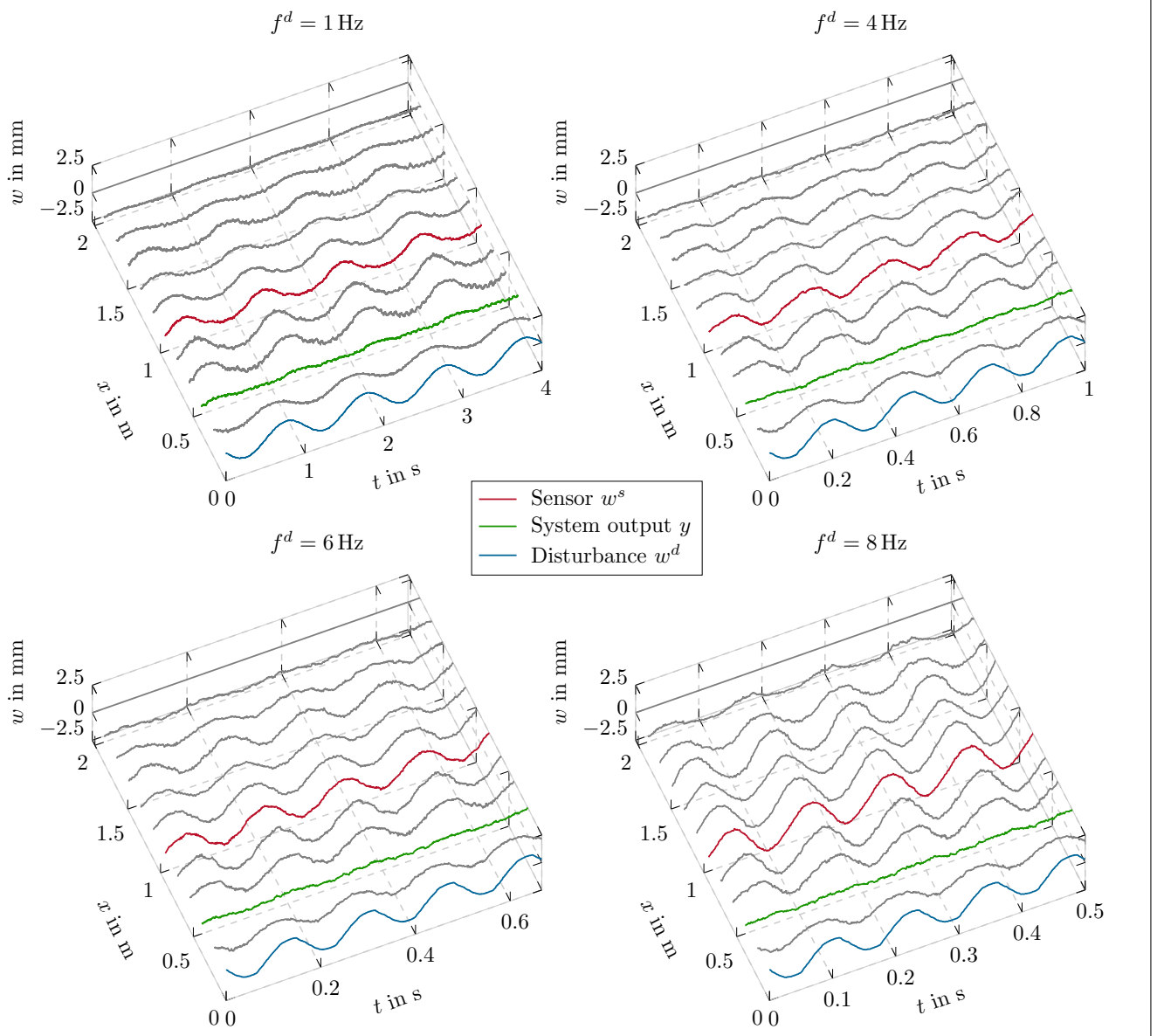

Figure 12: Measured strip displacement with active control: blue line - disturbance w^d with the amplitude 1 mm and different frequencies f^d; red line - sensor signal w^s used in the control concept; green line - system output y to be controlled; grey lines - measured displacements for validation purpose.

Post-print version of the article: M. Saxinger, L. Marko, A. Steinboeck, and A. Kugi, "Active rejection control for unknown harmonic disturbances of the transverse deflection of steel strips with control input, system output, sensor output, and disturbance input at different positions", *Mechatronics*, vol. 56, pp. 73–86, 2018, ISSN: 0957-4158. DOI: 10.1016/j.mechatronics.2018.10.008
The content of this post-print version is identical to the published paper but without the publisher's final layout or copy editing.

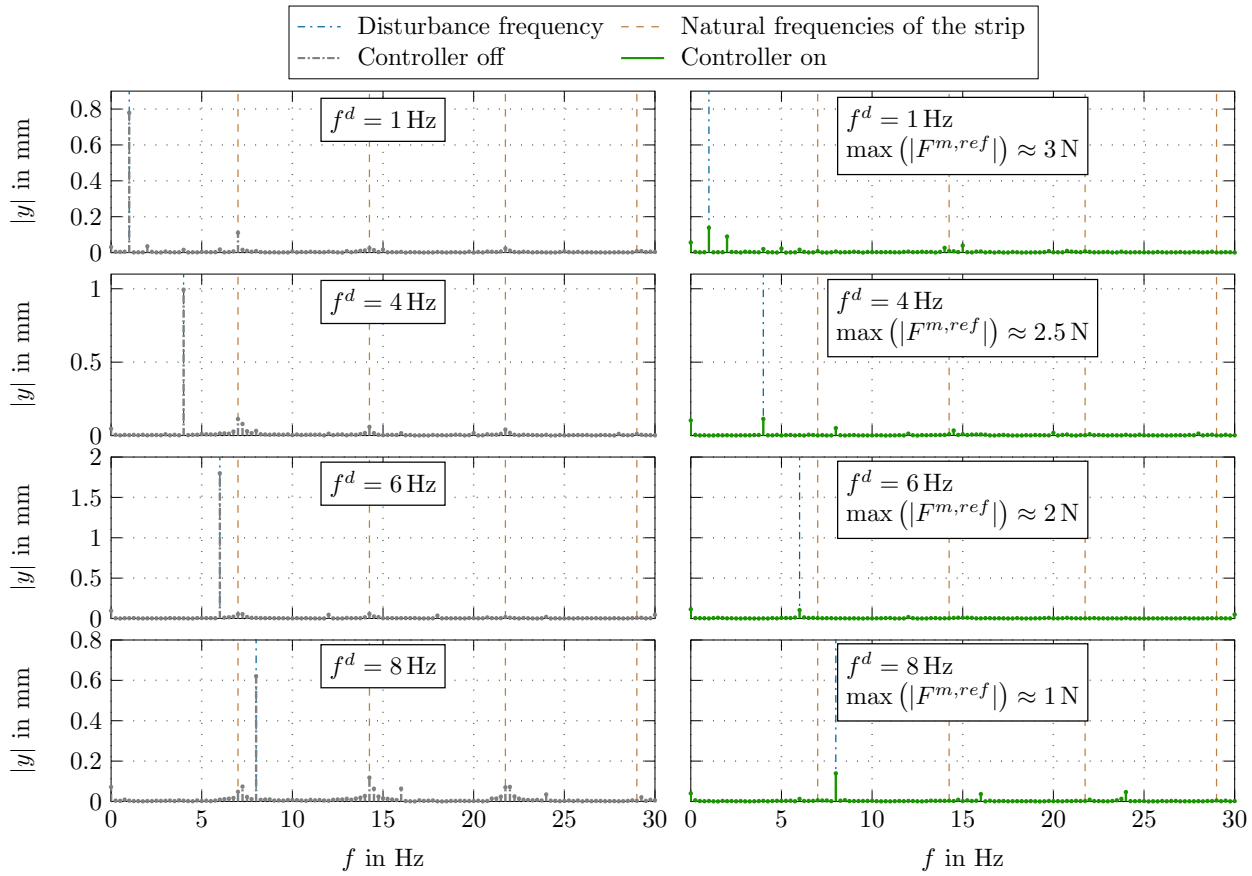

Figure 13: Spectra of measured displacement signals without and with control for different disturbance frequencies f^d.

Post-print version of the article: M. Saxinger, L. Marko, A. Steinboeck, and A. Kugi, "Active rejection control for unknown harmonic disturbances of the transverse deflection of steel strips with control input, system output, sensor output, and disturbance input at different positions", *Mechatronics*, vol. 56, pp. 73–86, 2018, ISSN: 0957-4158. DOI: 10.1016/j.mechatronics.2018.10.008
The content of this post-print version is identical to the published paper but without the publisher's final layout or copy editing.

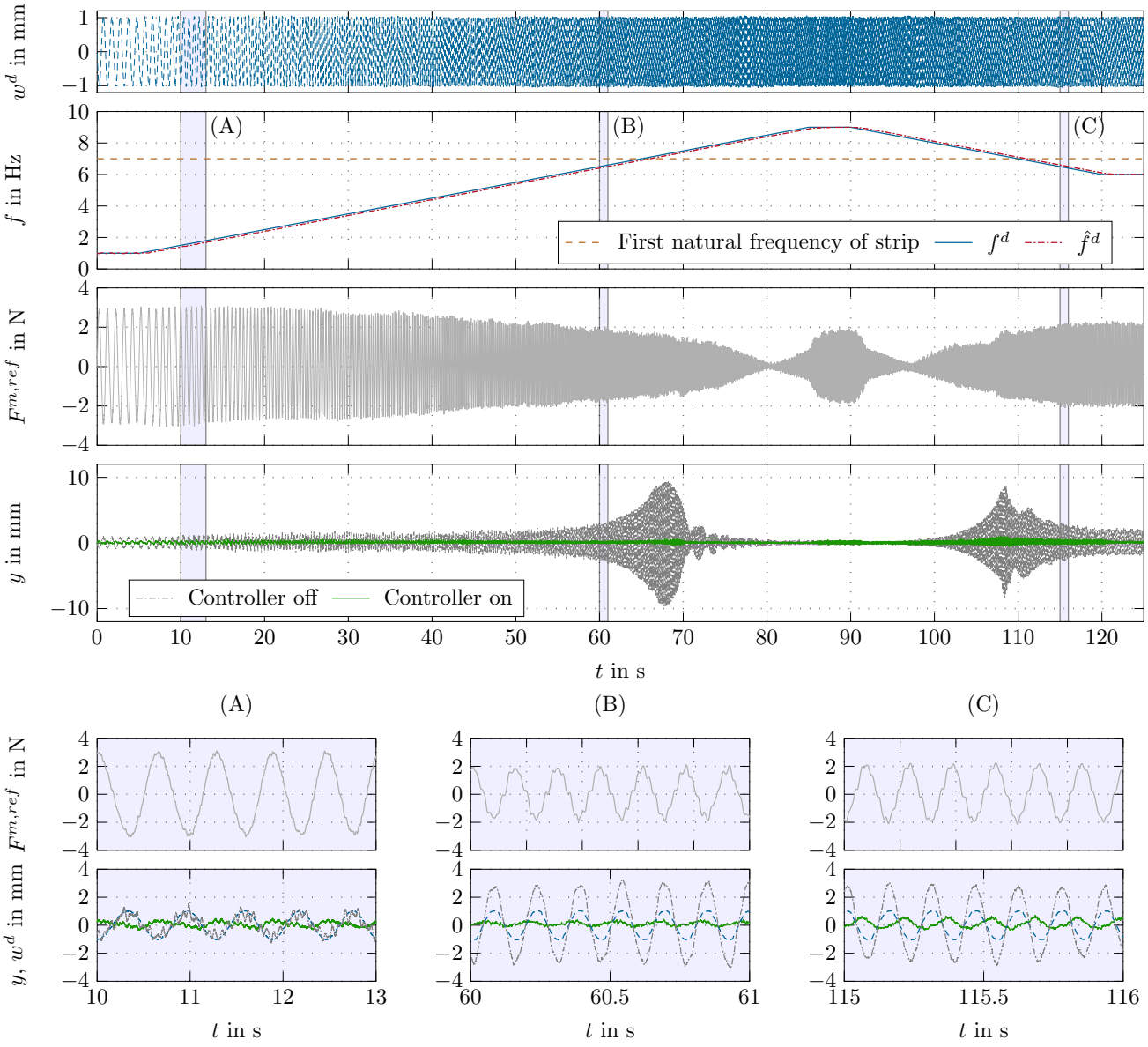

Figure 14: Experimental results for a slowly changing disturbance frequency.

Post-print version of the article: M. Saxinger, L. Marko, A. Steinboeck, and A. Kugi, "Active rejection control for unknown harmonic disturbances of the transverse deflection of steel strips with control input, system output, sensor output, and disturbance input at different positions", *Mechatronics*, vol. 56, pp. 73–86, 2018, ISSN: 0957-4158. DOI: 10.1016/j.mechatronics.2018.10.008
The content of this post-print version is identical to the published paper but without the publisher's final layout or copy editing.